GA Technologies

GA-C18103

FORT ST. VRAIN CYCLE 3
CORE PERFORMANCE

Work Done By:
FSV Engineering Staff

Report Written By:
R. Hackney

GA TECHNOLOGIES PROJECT 1900
November 1985

ABSTRACT

The Fort St. Vrain (FSV) Nuclear Generating Station, owned and operated by Public Service Company (PSC) of Colorado, is a plant employing the high-temperature gas-cooled reactor (HTGR) concept. Initial criticality was achieved in January 1974 and cycle 1 operation continued through February 1979. Throughout cycle 1 operation the maximum power was limited, by license restrictions, to 589 MW(t) or 70% of full power. Cycle 1 core performance was, in general, close to predictions. One exception to this good agreement with expected performance was the region exit gas temperature fluctuations which were detected early in the cycle. At the end of cycle 1 operation, the cause of the fluctuations was not positively identified but the most likely explanation was small movements of reactor components such as fuel elements, reflector elements, and/or core support floor.

The first refueling was completed in April 1979, and initial criticality of the cycle 2 core occurred in May 1979. The core was then operated at power levels up to 70% of rated power until October 1979 when the plant was shut down for installation of region constraint devices (RCDs). These RCDs were installed to stabilize gap flow areas at the top of the core to near nominal values so as to minimize block movement and, therefore, eliminate the temperature fluctuations. Cycle 2 operation continued at power levels up to 70% of rated power with core performance as predicted and no fluctuations were detected. In March 1981, the Nuclear Regulatory Commission (NRC) issued a release to test above 70% power. These tests demonstrated successful operation up to 90% of rated power before the testing was terminated for plant maintenance and for the second refueling.

Initial criticality of the cycle 3 core occurred in July 1981. Testing in the fall of 1981 demonstrated successful operation, without fluctuations, at power levels up to 100% of rated power and at pressure drops up to 5.0 psid. Results of these tests led to the NRC release, in October 1982, for 100% rated power operation. Cycle 3 operation continued until January 1984 when the plant was shut down for the third refueling. Throughout the cycle the core performance was, in general, as predicted.

This report discusses the core performance during cycle 3 operation.

ACRONYMS

APF	Axial power factor
BISO	Two-coating fuel particle
BOC	Beginning-of-cycle
BOL	Beginning-of-life
BWR	Boiling water reactor
CSB	Core support block
DL	Data logger
DOE	Department of Energy
EFPD	Effective full power day
EOC	End-of-cycle
FDDM	Fuel Design Data Manual
FIMA	Fissions per initial heavy metal atom
FSV	Fort St. Vrain
FTE	Fuel test element
GA	GA Technologies
HEU	High enriched uranium (93% U-235)
HSF	Hot service facility
HTGR	High-temperature gas-cooled reactor
ICRD	Instrumented control rod drive
LBP	Lumped burnable poison
LCO	Limiting condition for operation
LWR	Light-water reactor
MEU	Medium enriched uranium
MOC	Middle-of-cycle
MWd	Megawatt day
NRC	Nuclear Regulatory Commission
NW	Northwest
PCRV	Prestressed concrete reactor vessel
PIE	Post irradiation examination

PPS	Plant protective system
PSC	Public Service Company of Colorado
PWR	Pressurized water reactor
QC	Quality Control
R/B	Release/birth rate ratio
RCD	Region constraint device
RPF	Region (power) peaking factor
RSS	Reserve shutdown system
RT	Request for test
RWP	Rod withdrawal prohibit
SAR	Safety Analysis Report
S/N	Serial number
SOP	System Operating Procedure
SR	Surveillance requirement
TRISO	Four-coating fuel particle
WAR	Weak acid resin

CONTENTS

1. SUMMARY 1-1
2. CORE DESCRIPTION 2-1
3. POWER AND ENERGY HISTORY 3-1
4. NUCLEAR PERFORMANCE 4-1
   4.1. Initial Criticality 4-1
   4.2. Control Rod Group Reactivity Worth 4-1
   4.3. Temperature Defect 4-4
   4.4. Nuclear Detector Decalibration 4-4
   4.5. Fuel Accountability 4-7
      4.5.1. Heavy Metal Inventory 4-9
      4.5.2. Region Peaking Factors (Two Versus Three Dimensional Calculation) 4-9
      4.5.3. Fractional Absorptions and Excess Reactivity . . 4-11
      4.5.4. Particle Burnup 4-11
      4.5.5. Axial Power Data 4-13
      4.5.6. Power Correction Factors for Fuel Test Elements. 4-16
      4.5.7. Burnup Data for Cycles 1, 2, and 3 4-16
   4.6. Reactivity Discrepancy 4-16
   4.7. Control Rod Management 4-26
5. THERMAL/FLOW PERFORMANCE 5-1
   5.1. Region Peaking Factor 5-1
6. FUEL PERFORMANCE 6-1
   6.1. Calculational Methods 6-1
   6.2. Results 6-3
      6.2.1. Fuel and Graphite Temperature 6-3
      6.2.2. Fuel Particle Failure 6-6
      6.2.3. Gaseous Fission Product Release 6-10
      6.2.4. Metallic Fission Product Release 6-13
   6.3. Conclusions 6-17

7. SPECIAL TESTS AND SURVEILLANCES 7-1
7.1. Chemistry Surveillances 7-1
7.1.1. Coolant Impurities 7-1
7.1.2. Noble Gas Release/Birth (R/B) 7-1
7.1.3. Tritium Concentrations 7-2
7.1.4. Iodine Monitor 7-2
7.1.5. Plateout on Circulator 7-3
7.1.6. Gamma Activity of PGX Surveillance Samples . . . 7-3
7.1.7. Gamma Scanning of Circulator 7-3
7.2. Plateout Probe 7-4
7.3. Core Support Block Oxidation 7-5
7.4. PGX Graphite Surveillance 7-6
7.5. Fuel Test Elements 7-7
7.6. Post Irradiation Examination of Fuel and Reflector Elements 7-8
7.6.1. Segment 2 Elements 7-8
7.6.2. Segment 3 Elements 7-10
7.7. Gamma Scanning of Fuel Elements 7-12
7.8. Scratcher Plenum Elements 7-12
7.9. Temperature Fluctuations 7-13
7.9.1. Background 7-13
7.9.2. Cycle 3 Testing 7-16
7.10. Radiation Exposure 7-17
8. UNUSUAL OCCURRENCES 8-1
8.1. Inadvertent Insertion of Reserve Shutdown Material into Region 27 8-1
8.2. Cracked Fuel Element Web 8-3
8.3. Power Level Uncertainty 8-3
9. REFERENCES 9-1

FIGURES

2-1. Cycle 3 core layout 2-2
3-1. Cycle 3 thermal power history 3-2
3-2. Cycle 3 thermal energy history 3-3
3-3. Cycle 3 thermal and electrical energy history 3-4
3-4. Cumulative thermal energy from BOL 3-5
3-5. Cumulative thermal and electrical energy from BOL 3-6
4-1. Cycle 3 temperature defect 4-5
4-2. Axial power distribution - FTE-2 4-17
4-3. Axial power distribution - FTE-3 4-18
4-4. Axial power distribution - FTE-4 4-19
4-5. Axial power distribution - FTE-5 4-20
4-6. Calculated minus measured K_{eff} 4-25
5-1. Comparison of measured and calculated RPF distribution . . . 5-4
6-1. Peak fuel C/L temperature distribution 6-4
6-2. Time averaged fuel C/L temperature distribution 6-5
6-3. Fast neutron fluence distribution 6-7
6-4. Failed particle percentage - fissile particle 6-8
6-5. Failed particle percentage - fertile particle 6-9
6-6. Comparison of measured and predicted Kr-85m release 6-11
6-7. Comparison of measured and predicted Kr-85m release 6-12

TABLES

2-1. Cycle 3 control rod withdrawal sequence 2-6
4-1. Comparison of measured and calculated control rod group reactivity worth 4-3
4-2. Comparison of measured and calculated detector decalibration for sequential control rod group withdrawal 4-8

4-3. Total core heavy metal inventory at EOC3 4-10
4-4. Maximum fissile particle FIMA 4-12
4-5. Axial power data at EOC3 4-14
4-6. Heavy metal core loadings for cycles 1, 2, and 3 4-21
4-7. Fractional fissions for cycles 1, 2, and 3 4-22
4-8. Segment burnup for cycles 1, 2, and 3 4-23
4-9. Fast neutron exposure of control rod clad 4-27
4-10. Thermal neutron exposure of control rod clad 4-29
4-11. Control rod burnup 4-31
6-1. Sr-90 release 6-14
6-2. Cs-134 release 6-15
6-3. Cs-137 release 6-16
7-1. Comparison of radiation history - FSV vs LWRs 7-18

1. SUMMARY

Initial criticality of the cycle 3 core occurred in July 1981. Prior to January 1984, when the plant was shut down for the third refueling, the cycle 3 core had operated for a total of 295* effective full power days (EFPDs). The cumulative burnup for fuel segments 3 through 6, at the end of cycle 3 was 658 EFPDs*.

During the initial cycle 3 rise to power, tests were conducted by PSC to verify that the core performance was as predicted. In addition, core performance data have been monitored throughout the cycle. Although much of these data have been previously reported (Refs. 1 through 8), this report summarizes the overall cycle 3 core performance.

The nuclear performance was, in general, as predicted. Reasonable agreement between measured and calculated data was obtained for the temperature coefficient and for control rod worths. Initial criticality and reactivity behavior with burnup was also predicted with reasonable accuracy.

The thermal/flow performance was basically unchanged from previous cycles. Significant region peaking factor (RPF) discrepancies continued to exist in the northwest boundary regions, the result of region exit temperature measurement errors due to cool gas flowing inside the thermocouple sleeve. In order to compensate for these measurement errors, Technical Specification Limiting Condition for Operation (LCO) 4.1.7 was revised to include special operating procedures.

---

*Throughout this report the burnup (in EFPDs) is given to the nearest whole number.

The fuel performance for previous cycles grossly overpredicted fuel failure. Therefore, the models were refined and all three cycles were re-evaluated resulting in generally good agreement between measured and calculated fuel performance data.

Further fluctuation testing demonstrated that the region constraint devices (RCDs) were successful in preventing temperature fluctuations at power levels up to 100% of rated power and at core pressure drops up to 5.0 psi. As a result of these tests, confirming resolution of the temperature fluctuations observed during cycles 1 and 2, the NRC approved unrestricted full power operation.

The overall core performance of cycle 3 was, in general, as expected.

2. CORE DESCRIPTION

The active core consists of six layers of fuel elements with 247 fuel elements per layer. The fuel elements are grouped into 37 separate refueling regions surrounded by a graphite reflector as shown in Fig. 2-1. Each of the 37 refueling regions consists of either five or seven fuel columns and contains an orifice flow control assembly and a pair of control rods.

The fresh fuel materials are high enriched uranium (HEU)* and fertile thorium in carbide form. The uranium and thorium carbide particles are coated with layers of pyrocarbon and silicon carbide and bonded into fuel rods within the hexagonal graphite elements. The particle coatings provide the prime barrier for fission product retention. The core is designed to produce 842 MW(t) at a power density of 6.3 kW(t)/liter.

The thorium/uranium fuel cycle specifies that approximately one-sixth of the core be replaced with fresh fuel at each refueling cycle. This means that six refueling regions are reloaded at each refueling except for the fifth reload, at which time the central refueling region is also replaced. Each reload segment consists of 204 standard fuel elements and 36 control rod fuel elements, except as noted for the fifth reload. In

---

*Isotopic content of uranium:

U-234	0.0073
U-235	0.9315
U-236	0.0028
U-238	0.0584
	1.0000

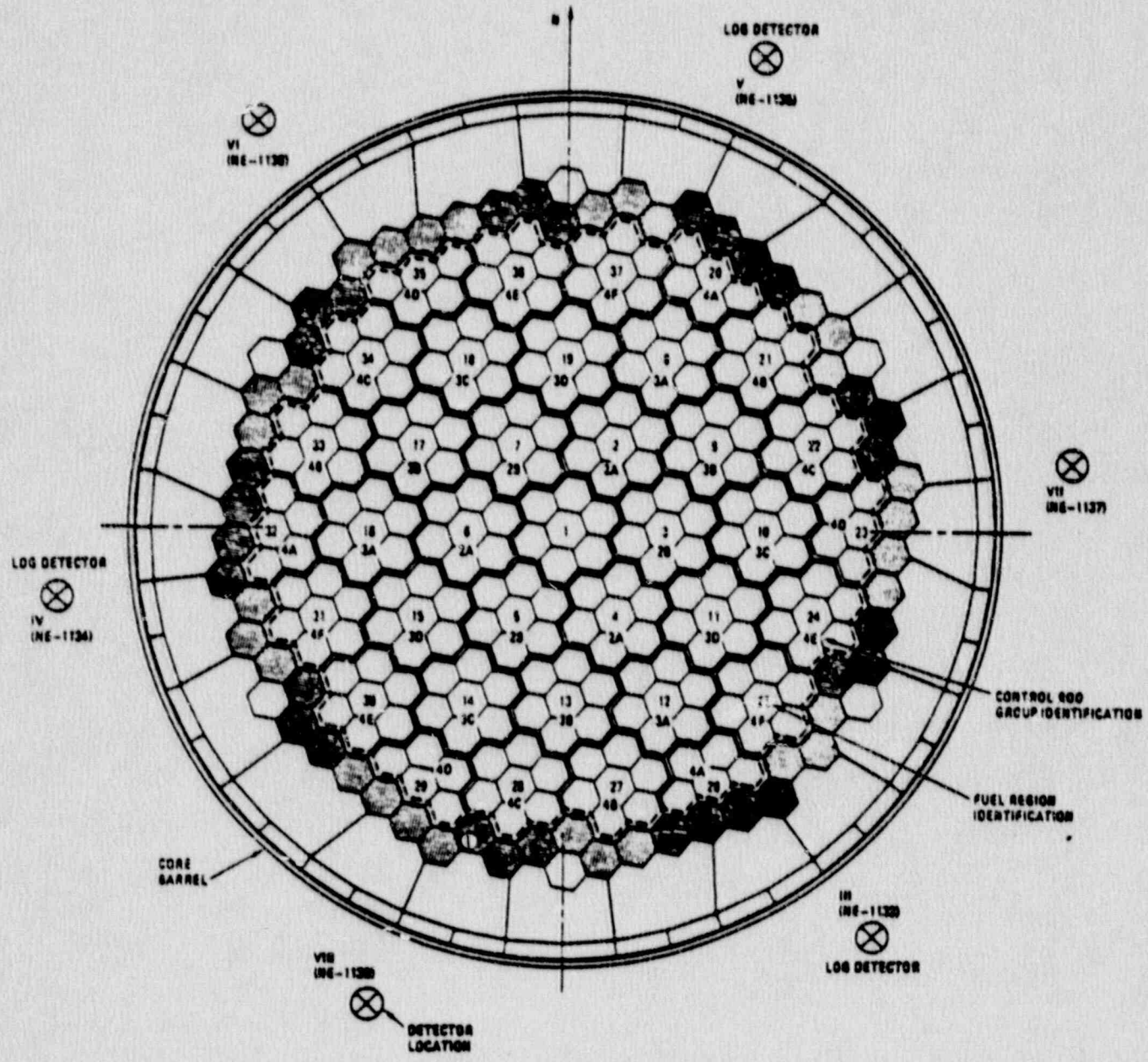

Fig. 2-1 FSV core layout and locations of ex-core detectors

each reload segment five of the refueling regions contain seven fuel columns and one contains five columns. The refueling region sequence was chosen so that freshly refueled regions are never adjacent to each other, except when the central region is refueled.

The reactor is controlled by a pair of cylindrical control rods in each of the 37 refueling regions, each with an independent control rod drive. A reserve shutdown system, in the form of B_4C graphite balls, is provided for backup shutdown capability.

The core power level is measured by six wide-range neutron flux detectors located symmetrically around the core, in the prestressed concrete reactor vessel (PCRV), at about the core midplane.

The core contains 84 region constraint devices (RCDs), installed in the core in late 1979 as a means of eliminating the temperature fluctuations. These RCDs mechanically interlock fuel regions at the top plenum layer of the core to prevent development of nonuniform clearance gaps between the internally keyed refueling regions. Details of the RCD design are given in Ref. 9.

Instrumented control rod drives (ICRDs) are located in refueling regions 5 (S/N 20) and 35 (S/N 43) to provide in-core data as an aid in understanding the fluctuation phenomenon. These ICRDs are standard control rod assemblies in which one control rod of the pair was removed and replaced with an instrument package. (These ICRDs were removed from the core at the end of cycle 3 and replaced with a standard control rod pair.)

Scratcher plenum elements are located above refueling regions 18 and 35 to permit measurement of relative motion between adjacent refueling regions. [These scratcher elements were removed at the end of cycle 3 (see Section 7.8).]

During the loading of segment 7 (reload 1), eight fuel test elements (FTEs), FTE-1 through FTE-8, were loaded into layer six of regions 25, 22, 30, 27, 24, 10, 5, and 5, respectively. (Details of the FTEs are given in Ref. 10.) These FTEs are intended to demonstrate acceptable performance and safety of proposed future FSV fuel and processes prior to full-scale application (see Section 7.5).

At the end of cycle 2 operation, segment 2 fuel was replaced with segment 8 fuel in refueling regions 4, 8, 15, 25, 32, and 36, i.e., the cycle 3 core contained fuel segments 3 through 8. The reloaded regions are shown as the shaded areas in Fig. 2-1. A detailed description of the segment 8 fuel design is given in Ref. 11.

Other differences between the cycle 3 and cycle 2 cores are discussed below:

- Segment 8 fuel fabrication differed from previous segments in that (1) leftover segment 7 fuel rods were used in some fuel elements, (2) several fuel rod lots contained high microporosity particles loaded in the bottom layer of the core, and (3) several elements with fuel rods containing uranium loadings higher than specified were loaded into special core locations (Ref. 12).

- Fuel elements with a "thin" buffer were replaced with a "thick" buffer, i.e., the entire fuel element (Ref. 11).

- A new concept for the lumped burnable poison (LBP) design was used in segment 8. This new concept used a single LBP type for all reloads. The LBP rods used in this new approach are shorter in length (-2 in.) than the previous designs which used 28-in. long LBP rods. The shorter length LBP rods are stacked along with "dummy" graphite spacer rods in a specified order into each LBP hole. (This design was modified slightly for segment 8 so

that leftover segment 7 LBP rods could be cut into approximately 2-in. lengths and used.) A description of the segment 8 fuel design and predicted performance is given in Refs. 11 and 13.

- The control rod withdrawal sequence was changed to maintain the maximum control rod worth and the region peaking factor requirements within LCO 4.1.3 limits. The withdrawal sequence is given in Table 2-1.

TABLE 2-1
CONTROL ROD WITHDRAWAL SEQUENCE

Control Rod Group	Regions
2B	3,5,7
4A	20,26,32
4C	22,28,34
1 (0 → 115 in.)	1
4E	24,30,36
4F	25,31,37
2A	2,4,6
4D	23,29,35
3A	8,12,16
3C	10,14,18
4B	21,27,33
3D	11,15,19
3B	9,13,17
1 (115 → 190 in.)	1

3. POWER AND ENERGY HISTORY

Cycle 3 operation began in July 1981. Prior to January 1984, when the plant was shut down for the third refueling, the cycle 3 core had operated for a total of 295 effective full power days (EFPDs). The cumulative burnup for fuel segments 3 through 6, at the end of cycle 3 was 658 EFPDs. The thermal energy generation for cycle 3 was 5.95 x 10^6 MWh(t) for a total of 13.3 x 10^6 MWh(t) since the beginning of life (BOL). The gross electrical energy generated during cycle 3 was 1.96 x 10^6 MWh(e) for a total of 4.29 x 10^6 MWh(e) from BOL. During cycle 3, 100% of rated power was achieved for the first time. The thermal power history throughout cycle 3 operation is shown in Fig. 3-1.

The thermal energy and EFPDs as a function of time in cycle 3 is shown in Fig. 3-2, and Fig. 3-3 shows the thermal and electrical energy throughout cycle 3. The thermal energy and EFPDs, as a function of time since the BOL, is shown in Fig. 3-4. Figure 3-5 shows the thermal and electrical energy history from BOL.

FORT ST. VRAIN OPERATION HISTORY

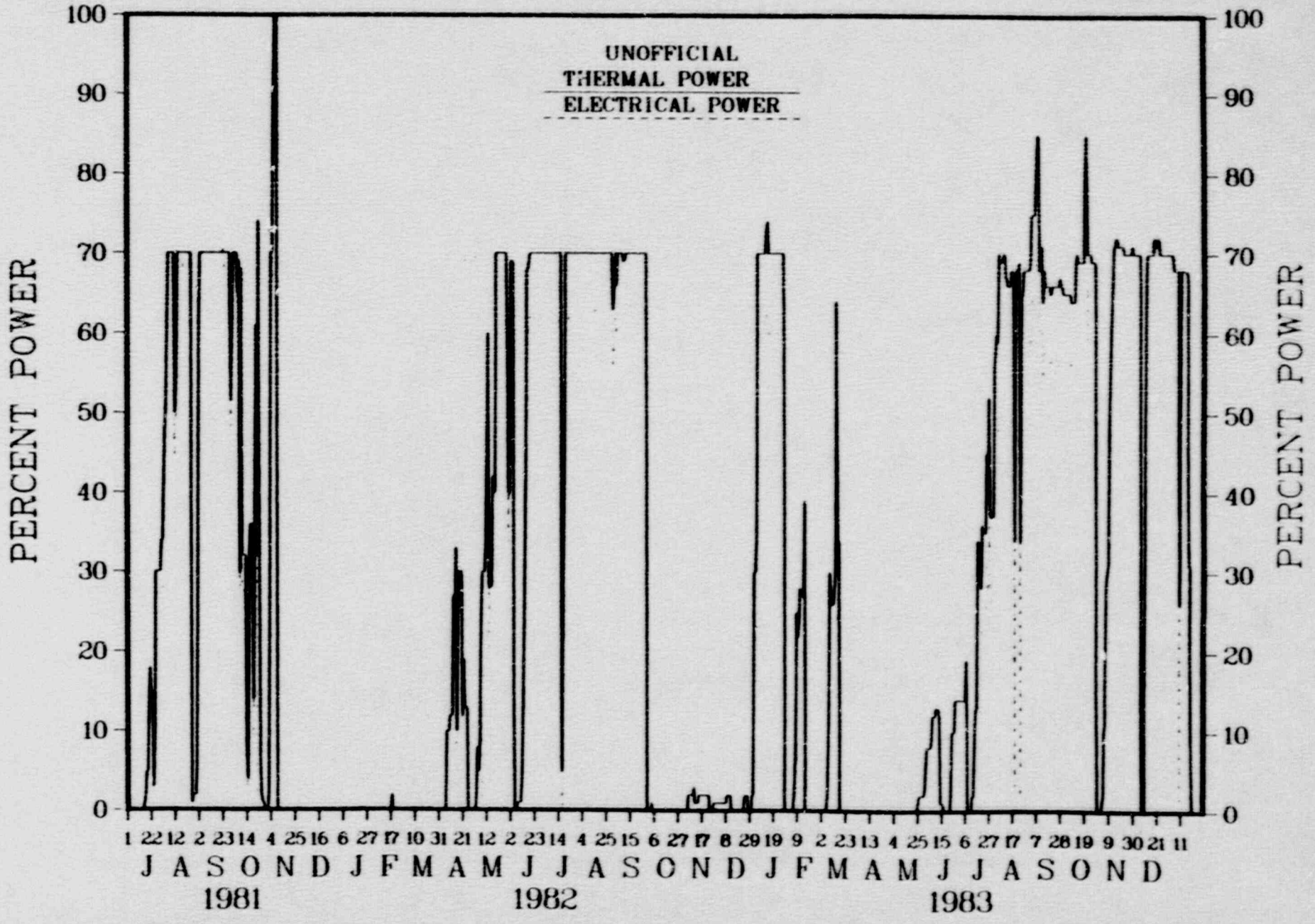

Fig. 3-1

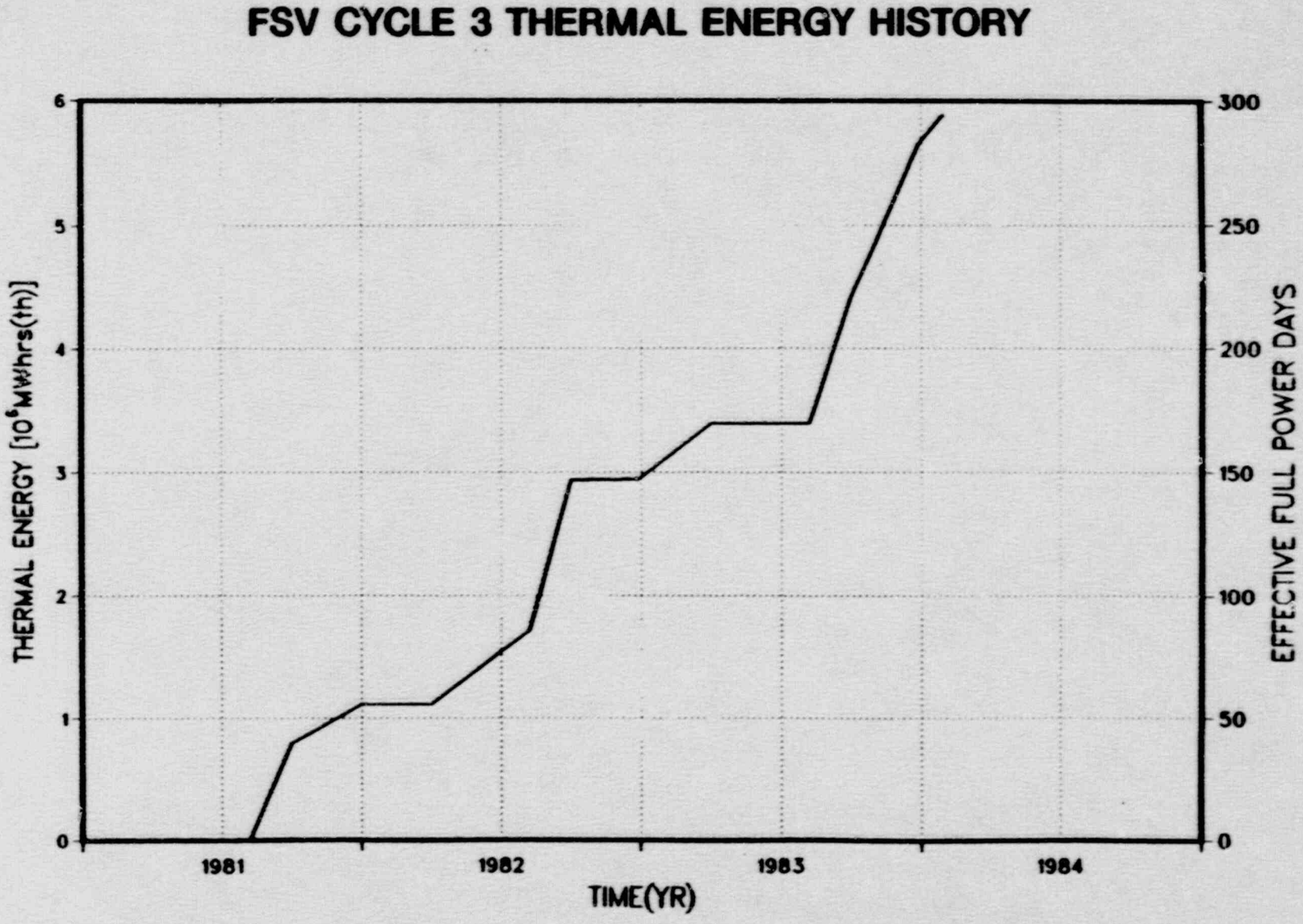
FSV CYCLE 3 THERMAL ENERGY HISTORY
THERMAL ENERGY [10⁶MWthrs(th)]
EFFECTIVE FULL POWER DAYS
TIME(YR)
0
1
2
3
4
5
6
0
50
100
150
200
250
300
1981
1982
1983
1984

Fig. 3-2

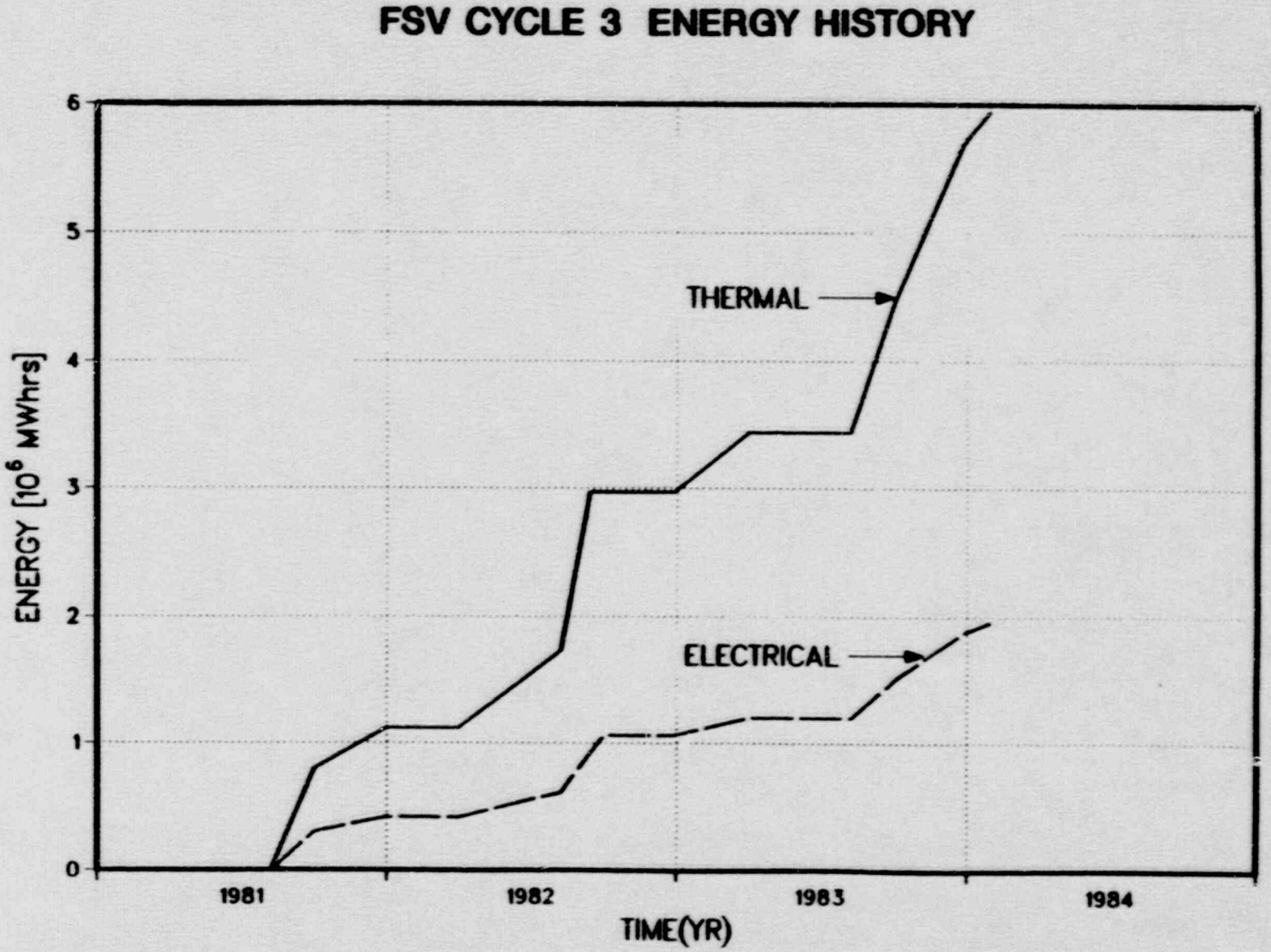
FSV CYCLE 3 ENERGY HISTORY
ENERGY [10^6 MWhrs]
0
1
2
3
4
5
6
THERMAL
ELECTRICAL
1981
1982
1983
1984
TIME(YR)

Fig. 3-3

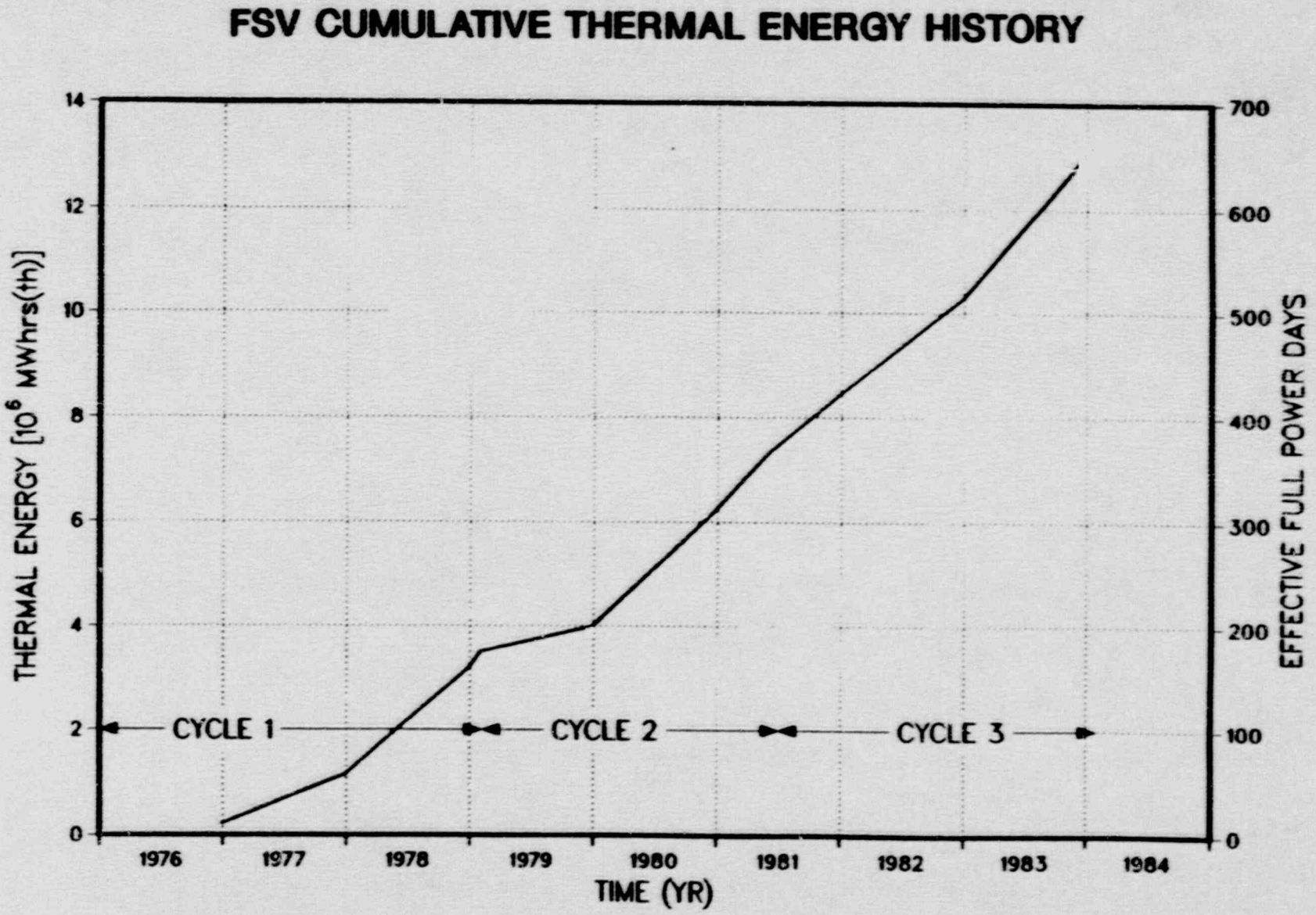
FSV CUMULATIVE THERMAL ENERGY HISTORY
THERMAL ENERGY [10^6 MWhrs(th)]
EFFECTIVE FULL POWER DAYS
0
2
4
6
8
10
12
14
0
100
200
300
400
500
600
700
CYCLE 1
CYCLE 2
CYCLE 3
1976
1977
1978
1979
1980
1981
1982
1983
1984
TIME (YR)

Fig. 3-4

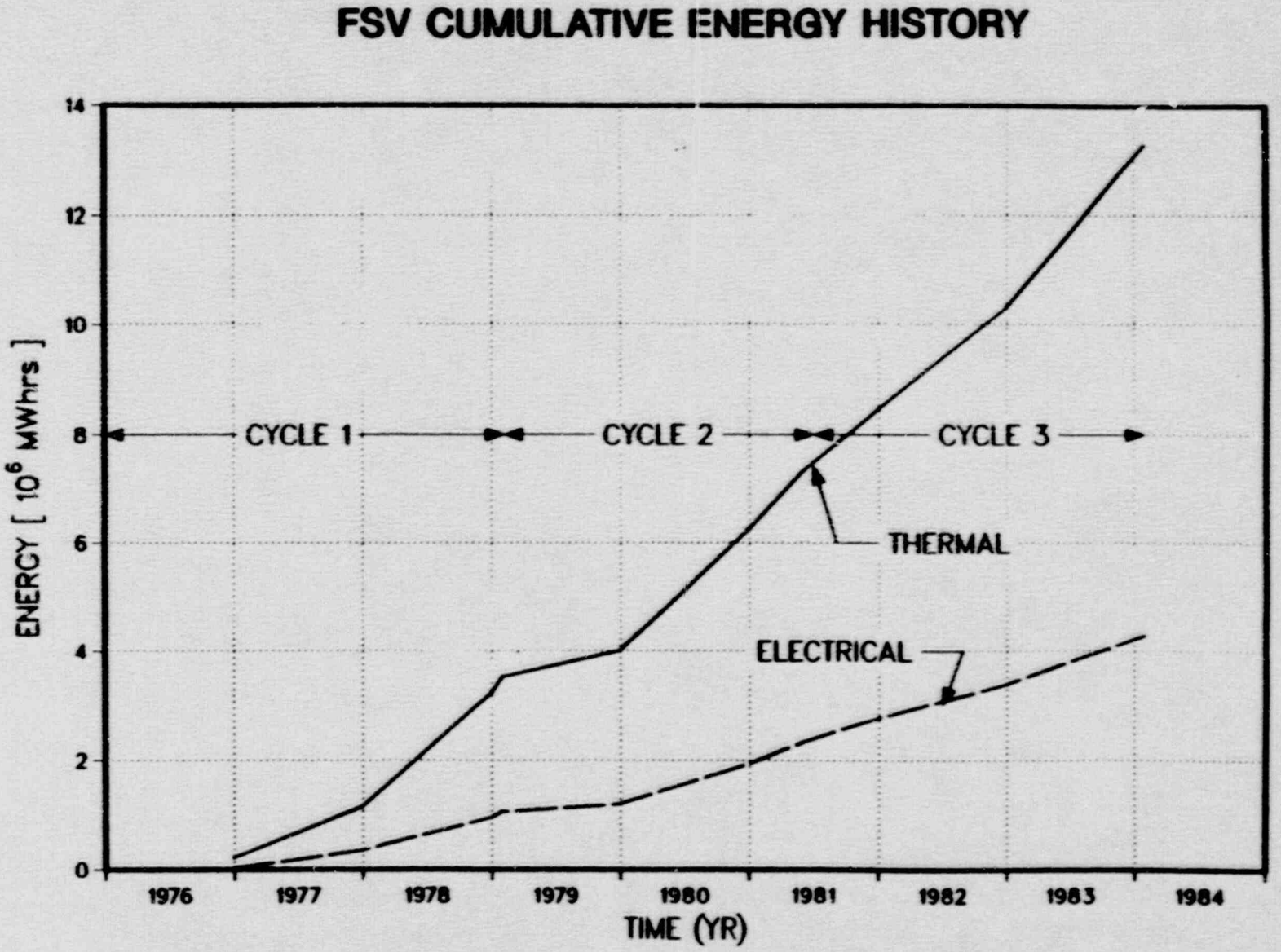
FSV CUMULATIVE ENERGY HISTORY
ENERGY [10^6 MWhrs]
14
12
10
8
6
4
2
0
CYCLE 1
CYCLE 2
CYCLE 3
THERMAL
ELECTRICAL
1976
1977
1978
1979
1980
1981
1982
1983
1984
TIME (YR)

Fig. 3-5

4. NUCLEAR PERFORMANCE

The following sections discuss the nuclear performance of the cycle 3 core.

4.1. INITIAL CRITICALITY

Initial criticality at the beginning of cycle 3 (BOC3) was achieved on July 15, 1981. The critical rod position was 99 in. on control rod group 4F. The average temperature was estimated to be about 230°F.

Initial "cold" criticality was calculated with the two-dimensional GAUGE model (Ref. 14). The effective multiplication factor calculated with the 4-group version was 0.9992, and with the 7-group version was 1.0060. A review of GAUGE model calculational reactivity bias* for the 7-group version at the end of cycle 2 indicated that the bias was 0.0065 ± 0.0015 Δk (Ref. 15). The calculational reactivity bias at the beginning of cycle 3 was essentially the same as during cycle 2 operation, indicating that the core behavior was as expected.

4.2. CONTROL ROD GROUP REACTIVITY WORTH

Surveillance specification SR 5.1.5 requires measurement of the reactivity worth of control rod groups as they are withdrawn from low power to the operating conditions at the beginning of each refueling cycle. The method used for measurement of control rod reactivity worth during cycle 3

---

*Reactivity bias is defined as the difference between the calculated k_{eff} and unity (the measured k_{eff}).

was the same as that used during the initial rise to power for cycles 1 and 2. The calibration technique, partially developed during the operation of the Peach Bottom HTGR, is referred to as the double-bump technique. An extension of the method was developed during FSV cycle 1 operation and is referred to as the substitution technique.

These calibration techniques have made use of an analog reactivity computer with input from the average of three of the plant nuclear detectors located outside the core at the midplane in the PCRV. The double-bump technique makes use of data obtained from the reactivity computer (and rod position indication) as any control rod is steadily withdrawn a distance of approximately 5 in. (or a reactivity worth of between five and ten cents)* and then immediately reinserted the same distance. The opposite motion was also used. The double-bump technique essentially eliminates the effect of temperature feedback on the measurement and can thus be performed during operation. These measurements provide differential rod (or group) reactivity worths ($\Delta\rho$/inch) at various control rod positions. A least squares polynomial fit was then made to the measured data to obtain the differential worth as a function of withdrawal distance.

Reactivity worth measurements, for control rod groups 4F, 2A, 4D, and 3A were made by PSC during the initial cycle 3 rise-to-power, i.e., from 2% to 65% power. Calculated control rod group worths were obtained using the GAUGE code where control rod groups were withdrawn, in sequence, at the beginning of cycle 3. The calculated data are reported in Ref. 16.

Table 4-1 shows a comparison of the measured and calculated integral reactivity worth for the four control rod groups measured. It is seen that the agreement between the measured and calculated integral worth is within

---

*One cent (1 ¢) is equivalent to a $\Delta\rho$ of -5.5×10^{-5} at BOC3 and -4.8×10^{-5} at EOC3.

TABLE 4-1
COMPARISON OF MEASURED AND CALCULATED
CONTROL ROD GROUP REACTIVITY WORTH

Control Rod Group	Integral Worth ($\Delta\rho$)		
	Measured	Calculated	% Difference*
4F	0.0220	0.0237	7.2
2A	0.0187	0.0183	-2.2
4D	0.0063	0.0064	1.6
3A	0.0170	0.0183	7.1
Total	0.0640	0.0667	4.0

*$[(\Delta\rho_{calc} - \Delta\rho_{meas})]/\Delta\rho_{calc}] \cdot 100.$

approximately 7% for any single group, while the difference between the measured and calculated cumulative worth is only approximately 4% (0.001 $\Delta\rho$).

These data are consistent with cycle 1 and 2 data in that the cumulative integral worths are predicted within a few percent while individual rod groups are predicted with somewhat less accuracy (Refs. 17 and 18). All measured rod group worths are, however, within the acceptance criterion specified for the test.

4.3. TEMPERATURE DEFECT

Surveillance requirement SR 5.1.3 specifies that a measurement of the reactivity change as a function of fuel temperature be made at the beginning of each refueling cycle. These measurements were performed by PSC during the initial cycle 3 rise-to-power.

The temperature defect was calculated using the 7-group GAUGE model as described in Ref. 16.

Figure 4-1 shows a comparison of the measured and calculated temperature defect. It is seen that the measured temperature defect, from 220°F to 1500°F, is approximately 6% lower than the calculated. This is consistent with cycle 1 and 2 data and within the expected range.

4.4. NUCLEAR DETECTOR DECALIBRATION

Power-range nuclear detector signals are used to monitor core power during steady state and transient conditions and in the automatic control system to initiate plant protection (PPS) action.

During cycle 1 and 2 operation, significant decalibration of these power range detectors, due to motion of control rod groups, was predicted and measured. This decalibration results from the location of the six

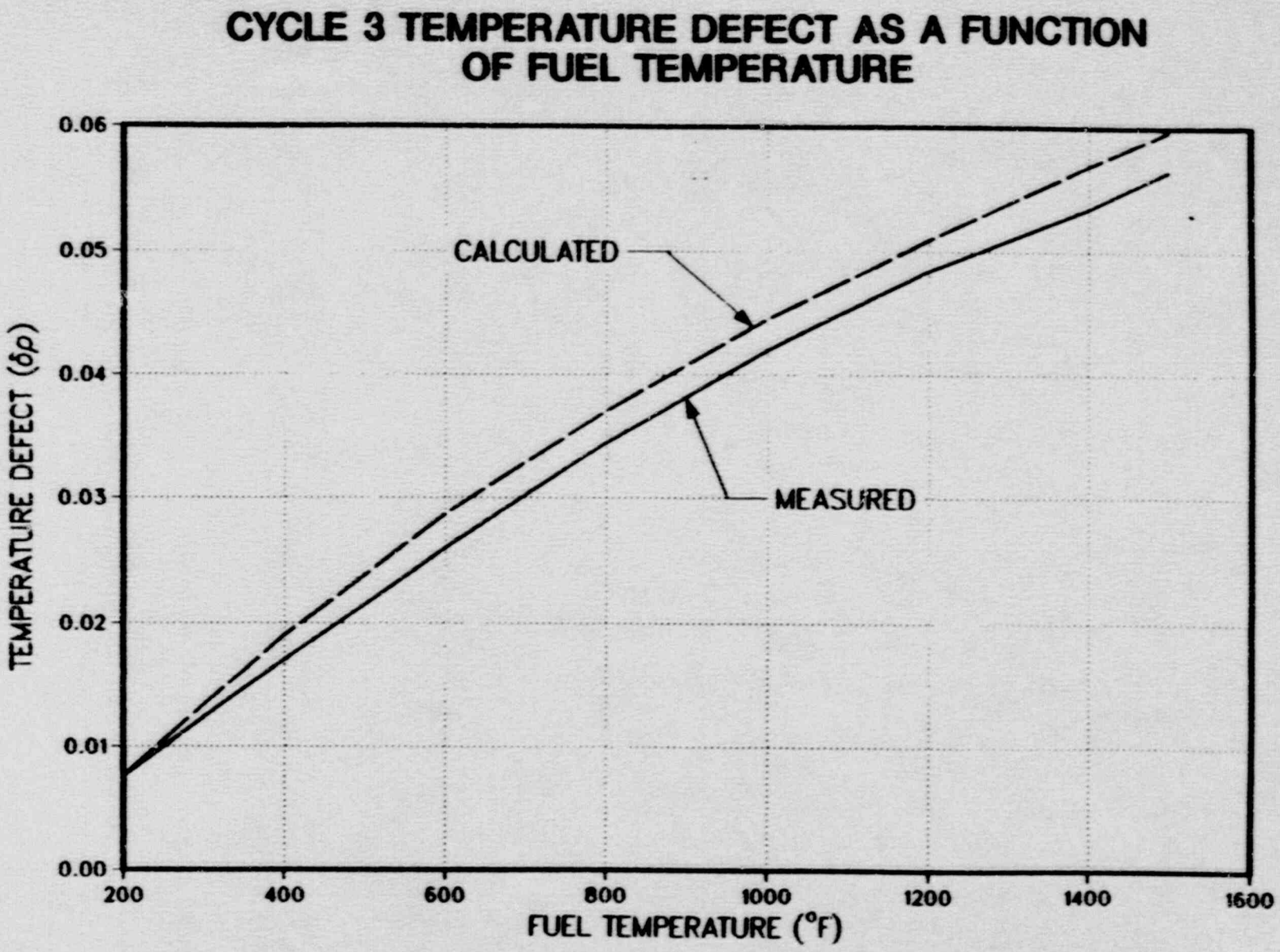
CYCLE 3 TEMPERATURE DEFECT AS A FUNCTION OF FUEL TEMPERATURE
TEMPERATURE DEFECT (δρ)
0.06
0.05
0.04
0.03
0.02
0.01
0.00
CALCULATED
MEASURED
200
400
600
800
1000
1200
1400
1600
FUEL TEMPERATURE (°F)

Fig. 4-1

detectors symmetrically around the core, in the PCRV (see Fig. 2-1). This means that each detector "sees" neutrons from principally a few fuel columns near the core boundary. Thus, changes in the distribution of power throughout the core, due to control rod position changes, can cause the detector signal to change more or less than the corresponding actual change in total core power. As a result of this detector decalibration, a "floating" trip point was recommended to assure the reactor trips at or below 140% thermal power (Ref. 19). The floating trip point hardware is not yet installed so the detector decalibration is accommodated by a reduction in the fixed PPS trip setpoints and frequent calibration of the nuclear channels. The fixed PPS setpoints are intended to activate a rod withdrawal prohibit (RWP) at 120% of rated power and to ensure that a reactor trip is always initiated before true power reaches the trip point of 140% rated power as required by the Technical Specifications.

Because of the different control rod withdrawal sequence in cycle 3 and the different core fuel loading distribution, it was necessary to re-evaluate the detector decalibration. Results of these detector decalibration analyses are reported in Ref. 16. Basically, the detector decalibration, i.e., the ratio of the detector indicated power level to the true power (heat balance), is calculated using the GAUGE code (Ref. 14) along with influence coefficients representing the contribution of adjacent columns to each detector response. Fixed PPS trip setpoints as a function of power were specified for cycle 3 operation, based on these analyses.

Measurements made by PSC during December 1983, using test procedure T-174, provided data on the measured detector decalibration for verification of these fixed trip setpoints. The voltage to each of the six linear channels was measured and this voltage is proportional to reactor power. Valid measured data were obtained for only two control rod groups (3C and 4B) as the groups were fully withdrawn. A re-calibration of the detectors was performed both before and after each rod group withdrawal. The measured decalibration factors were then defined as the ratio of the voltage before calibration to the voltage after calibration.

Table 4-2 gives a comparison of the measured and calculated detector decalibration factors for sequential withdrawal of control rod groups 3C and 4B. It is seen that the measured detector decalibration factors are generally lower than the calculated for rod group 3C and higher than the calculated for rod group 4B.

The worst case decalibration factor (decalibration which most delays the PPS trip) is typically calculated to occur when a control rod group is inserted after a control rod pair runs out. The calculated decalibration factor for the rod pair out was combined with the measured decalibration factor for the group insertion to determine the worst case decalibration factor for control rod groups 3C and 4B. Then, assuming opposite detectors are grouped and the signals auctioneered, and assuming that one channel fails in a nontripped mode (a conservative assumption since this is a two-out-of-three channel logic) the worst case decalibration factor determines the fixed PPS setpoint which will ensure a trip before the true power exceeds 140% of rated power. Comparison of this worst case decalibration with that using all calculated data indicated only a slightly lower setpoint for control rod group 4B. However, the specified reduced PPS fixed setpoints were determined from rod groups which cause significantly more decalibration than groups 3C and 4B.

Therefore, based on the limited valid measured data, there is no indication that the PPS setpoints based on calculated data are not valid. However, the valid measured data are for control rod groups which do not cause a significant delay in the PPS trip and, therefore, do not determine the PPS fixed reduced setpoints.

4.5. FUEL ACCOUNTABILITY

Fuel accountability calculations are done semiannually using the three-dimensional, 4-group CATT model (Ref. 20). These analyses provide fuel composition accountability information on a fuel element basis,

TABLE 4-2
COMPARISON OF MEASURED AND CALCULATED
DETECTOR DECALIBRATION FOR SEQUENTIAL CONTROL ROD
GROUP WITHDRAWAL

Nuclear* Channel	Control Rod Group 3C			Control Rod Group 4B		
	Meas.**	Calc.	Meas./Calc.	Meas.***	Calc.	Meas./Calc.
III	0.70	0.81	0.86	1.04	1.07	0.97
IV	0.73	0.81	0.90	1.09	1.00	1.09
V	0.82	0.82	1.00	1.11	1.04	1.07
VI	1.12	1.17	0.96	0.95	0.98	0.97
VII	1.06	1.18	0.90	1.19	0.99	1.20
VIII	1.01	1.23	0.82	1.01	1.03	0.98
Ave.	0.91	1.00		1.07	1.02	

*See Fig. 2-1 for nuclear channel location

**Using linear channel voltage - variation in linear channel power too large to be valid.

***Using linear channel voltage - linear channel V power not valid at 190 in.

including accountability information for the fuel in the fuel test elements (FTEs). Since GATT calculations are quite costly, the actual operating power history is modeled with only a few time steps. (The modeling of the complete cycle 3 power history is given in Ref. 21.) Then, a 7-group, two-dimensional GAUGE model is used to model the power history and to check the more complicated GATT analysis. Comparisons of the end of cycle (EOC) "total core" results from the two calculations models are discussed in Ref. 22 and summarized below. [The detailed information for each fuel element is stored on magnetic tape (Ref. 23).]

4.5.1. Heavy Metal Inventory

The heavy metal inventory of the core at the end of cycle 3 (EOC3) from the two calculational models is given in Table 4-3. The inventory from the GATT model is slightly (0.01%) less than that from the GAUGE model. This is primarily because the GAUGE model does not model the FTEs, whereas the GATT model represents them explicitly. Note that with about the same Th-232 and Pa-233 inventories in both models, the GAUGE model is consistently higher in U-233 content but is lower in U-235 content by about the same amount. Furthermore, the inventory of U-234 is higher in the GATT model as if the capture cross section of U-233 is also higher. The reason for this discrepancy is not known, but since U-233 is more reactive than U-235, the lower inventory of U-233 explains the lower reactivity of the GATT model (see Section 4.5.3). The difference between the total core inventory calculated with GAUGE and GATT is essentially the same as during the previous cycles.

4.5.2. Region Peaking Factors (Two- versus Three-Dimensional Calculation)

Comparisons of the region peaking factor (RPF) distribution from the GAUGE and GATT calculations were made throughout the cycle and, in general, the differences were small (approximately 4% to 5%). Somewhat larger differences may occur in partially rodded regions, due to the inability of the GATT model to represent control rods in any position other than by

TABLE 4-3
TOTAL CORE HEAVY METAL INVENTORY AT THE EOC3 (kg)

Nuclide	GAUGE	GATT
Th-232	14,509.35	14,508.58
Pa-233	17.09	17.01
U-233	215.27	208.36
U-234	21.86	23.04
U-235	410.35	415.84
U-236	89.02	87.92
U-238	51.12	51.06
Pu	3.15	3.23
Total	15,317.20	15,315.04

integer number of fuel layers, and to the apparent difference in the "S-curve" used in the GAUGE calculations and the one implicit in the GATT calculations. The "S-curve" used in GAUGE is based on measurements made at the beginning of cycle 3 and, therefore, does not account for the burnup effect throughout the cycle.

A discussion of the comparison of the RPF distributions from GAUGE and GATT is given in Ref. 22.

4.5.3. Fractional Absorptions and Excess Reactivity

The fractional absorptions by the major absorbers, the effective and infinite multiplication factors, and the total neutron leakage from the core calculated with the GAUGE and GATT models at the end of cycle 3 are compared in Ref. 22. The results were, in general, as predicted.

The total neutron leakage in GATT was somewhat higher than in GAUGE throughout the cycle. At the end of cycle 3 the difference reached about 0.003 Δk. Since GATT calculates the total leakage directly, while GAUGE relies on an estimated input value for the axial leakage, it is reasonable to conclude that this difference is real.

4.5.4. Particle Burnup

The maximum fissile particle fissions per initial heavy metal atom (FIMA), as a function of active core layer and reload segment, is given in Table 4-4. As previous analyses have shown, the maximum FIMA generally occurs in the fourth layer of the active core. The maximum burnup of any segment is about 658 EFPDs out of a potential total of approximately 1750 EFPDs, with the maximum fissile particle FIMA of 14.1% out of a projected 20% for the initial core segments. The maximum fertile particle FIMA was calculated to be 2.3% out of a projected 7%. The GATT results indicate that, in general, FIMAs increase somewhat faster with burnup than

TABLE 4-4
MAXIMUM FISSILE PARTICLE FIMA (%)

Core Layer	Reg. 1	Segs. 3-6	Seg. 7	Seg. 8
1 (top)	8	10	6	4
2	11	12	9	6
3	13	13	10	7
4	14	14	12	8
5	13	13	11	7
6	10	10	9	5

predicted with the GAUGE results based on the precalculated axial distribution profiles. However, for the present level of burnup the discrepancy is not significant.

4.5.5. Axial Power Data

The end of cycle GATT calculations were done with the control rod shim group 3D 66% withdrawn. The power fraction in the top half of the core, at the end of cycle, is shown in Table 4-5 for each region of the core. These results indicate that the power fraction in some of the older fuel regions is lower than the desired range of 0.55 to 0.60. However, this does not create a problem since the Technical Specification LCO 4.1.3 limits the magnitude of the axial power factor* (APF) in the bottom fuel layer. These APFs, also given in Table 4-5, indicate that the maximum unrodded region APF (region 30) is approximately 6% lower than the LCO limit of 0.90.

Although these data indicate a significant flattening of the axial power distribution with burnup and partial rod insertion, the fuel in the bottom core layer was depleted to such an extent that the power tilting toward the core bottom was mitigated and thus the LCO limits are met in every region with a substantial margin. However, by comparing the present results to those earlier in the cycle when the shim bank was 50% withdrawn, it is noted that the APFs at EOC3 are somewhat higher. This is contrary to the earlier projection that APFs had reached their highest levels, and that in the subsequent burnup an improvement in the core response to a partial control rod bank insertion would result. Therefore, a close monitoring of APFs in the next cycle is essential.

*Axial power factor is defined as the relative power in the bottom layer of a region to the relative power in the region.

TABLE 4-5
AXIAL POWER DATA AT EOC3

Region No.	Control Rod Insertion*	Power Fraction in Top Fuel Zone	APF in Bottom Block
1	2	0.464	0.838
2	0	0.518	0.765
3	0	0.516	0.788
4	0	0.543	0.724
5	0	0.550	0.738
6	0	0.611	0.781
7	0	0.514	0.776
8	0	0.564	0.678
9	6	0.543	0.726
10	0	0.563	0.707
11	2	0.472	0.818
12	0	0.527	0.743
13	6	0.545	0.725
14	0	0.522	0.758
15	2	0.490	0.808
16	0	0.522	0.748
17	6	0.580	0.686
18	0	0.539	0.721
19	2	0.476	0.817
20	0	0.540	0.713
21	0	0.589	0.645
22	0	0.548	0.706
23	0	0.532	0.740

*0 - Control rod fully withdrawn.
2 - Control rod inserted two core layers, i.e., withdrawn from four core layers.
6 - Control rod fully inserted.

TABLE 4-5 (Continued)

Region No.	Control Rod Insertion	Power Fraction in Top Fuel Zone	APF in Bottom Block
24	0	0.519	0.769
25	0	0.572	0.652
26	0	0.537	0.712
27	0	0.543	0.728
28	0	0.579	0.671
29	0	0.534	0.730
30	0	0.502	0.805
31	0	0.506	0.798
32	0	0.586	0.626
33	0	0.549	0.701
34	0	0.551	0.703
35	0	0.578	0.648
36	0	0.579	0.632
37	0	0.526	0.747
Average		0.535	0.733

4.5.6. Power Correction Factors for Fuel Test Elements

The axial power distribution in the columns containing fuel test elements (FTEs) was compared to the region average axial power distribution at EOC3. These data are shown in Figs. 4-2 through 4-5 for the columns containing FTEs 2 through 5. (The axial power distribution for the columns containing FTE-6, FTE-7, and FTE-8 are not given since these FTEs are essentially the same as the elements they replaced, i.e., only the type of graphite was changed and, therefore, the axial power distribution is essentially unchanged.) These results indicate that (1) the power generation of the FTEs is about 10% to 15% lower than in the element they replaced, and (2) the presence of FTEs has only a small effect on the axial power distribution in regions in which they are located and essentially no effect on the power distribution in adjacent regions. These data also illustrate the flattening of the axial power distribution and the increase in the APF in the bottom fuel layer that was discussed above.

4.5.7. Burnup Data for Cycles 1, 2, and 3

The heavy metal core loadings and the fractional fissions at the beginning and end of cycles 1, 2, and 3 are given in Tables 4-6 and 4-7, respectively. These data show that at EOC3 the net enrichment is approximately 80% with approximately 41% of the fissions occurring in U-233.

Table 4-8 shows the segment burnup at the end of cycles 1, 2, and 3. From these data it is seen that at EOC3 the maximum segment burnup was 36,417 MWd/tonne, and the core average burnup was 31,278 MWd/tonne.

4.6. REACTIVITY DISCREPANCY

The reactivity discrepancy, at any time during operation, is the reactivity difference between the critical position of the control rods and the critical position predicted for the specific operating conditions.

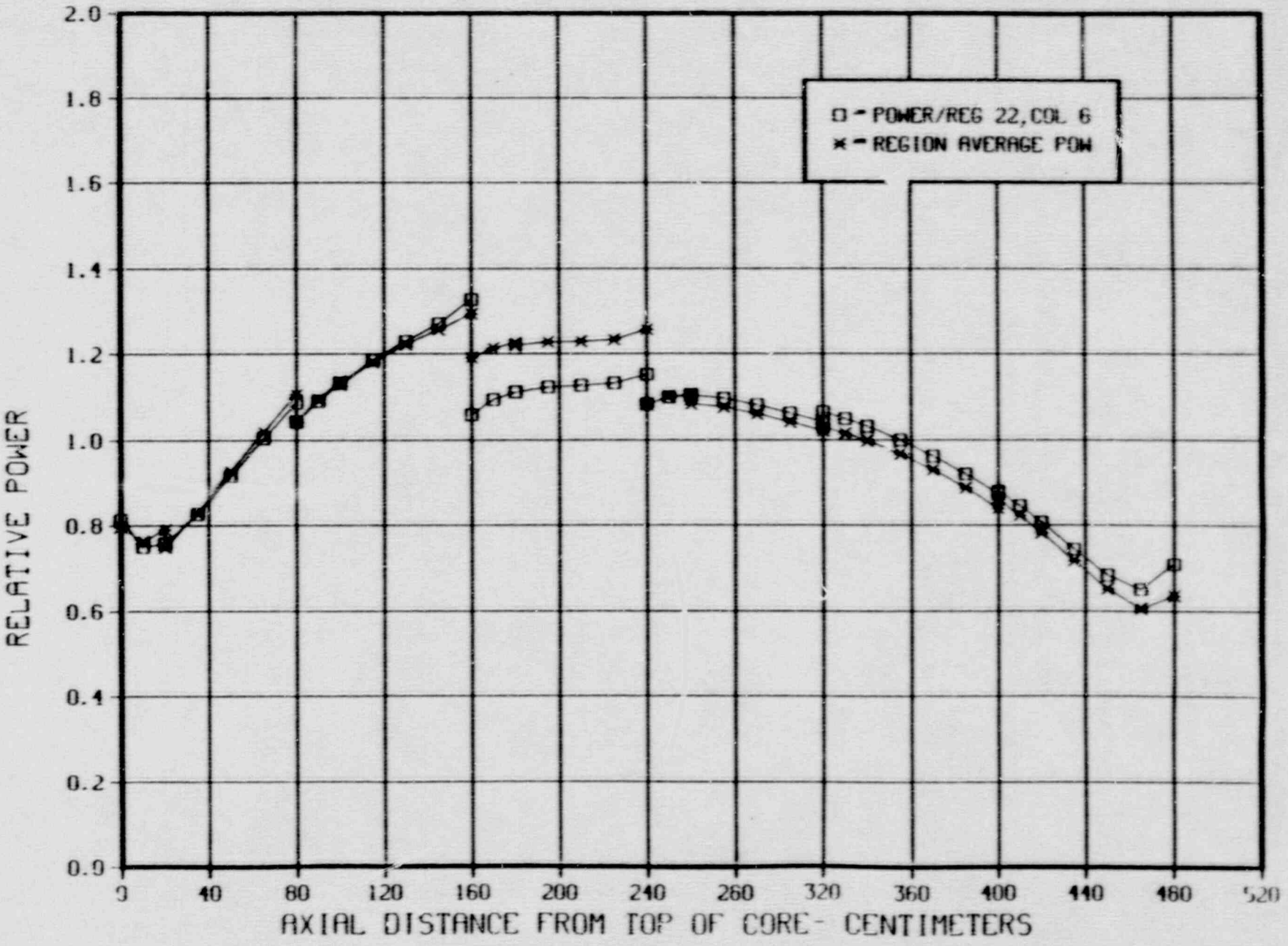
FSV -CYCLE 3- 294.5 EFPD - FTE-2 (22.06.F.06)
□ - POWER/REG 22,COL 6
* - REGION AVERAGE POW
RELATIVE POWER
2.0
1.8
1.6
1.4
1.2
1.0
0.8
0.6
0.4
0.2
0.0
3
40
80
120
160
200
240
280
320
360
400
440
480
520
AXIAL DISTANCE FROM TOP OF CORE- CENTIMETERS

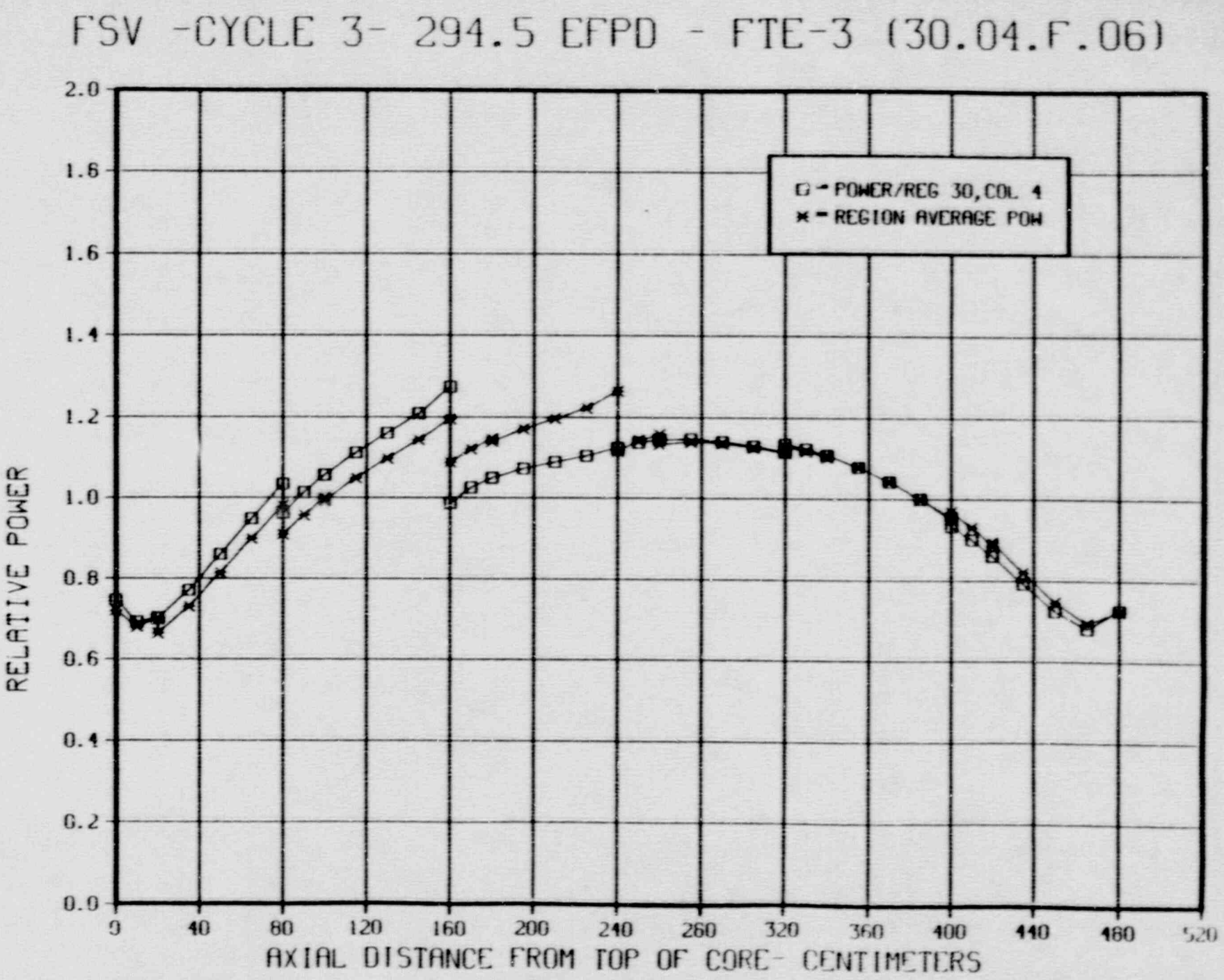
FSV -CYCLE 3- 294.5 EFPD - FTE-3 (30.04.F.06)
□ - POWER/REG 30,COL 4
* - REGION AVERAGE POW
RELATIVE POWER
AXIAL DISTANCE FROM TOP OF CORE- CENTIMETERS
2.0
1.6
1.6
1.4
1.2
1.0
0.8
0.6
0.4
0.2
0.0
0
40
80
120
160
200
240
280
320
360
400
440
480
520

Fig. 4-3

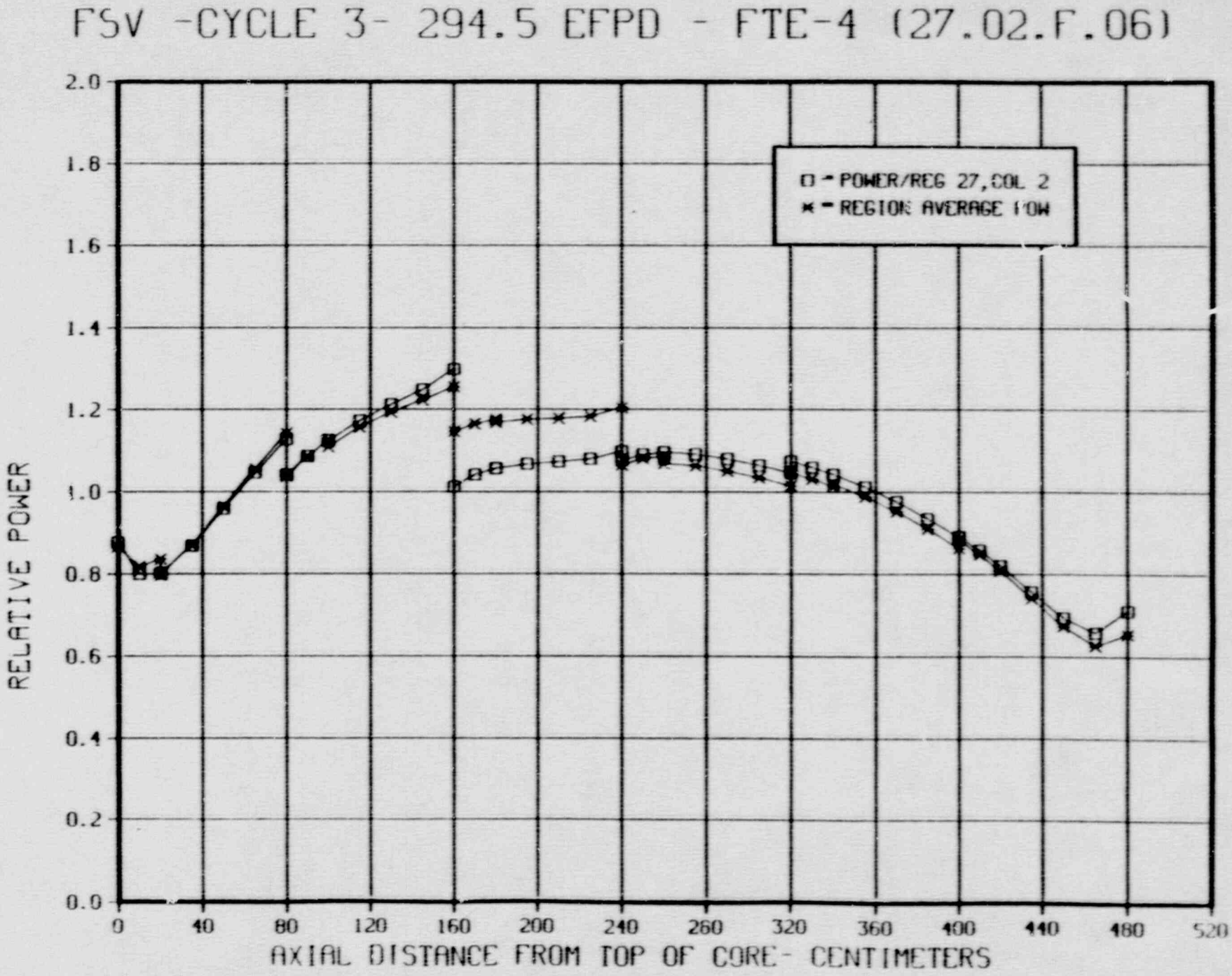
FSV -CYCLE 3- 294.5 EFPD - FTE-4 (27.02.F.06)
□ - POWER/REG 27,COL 2
× - REGION AVERAGE FOW
RELATIVE POWER
2.0
1.8
1.6
1.4
1.2
1.0
0.8
0.6
0.4
0.2
0.0
0
40
80
120
160
200
240
280
320
360
400
440
480
520
AXIAL DISTANCE FROM TOP OF CORE- CENTIMETERS

Fig. 4-4

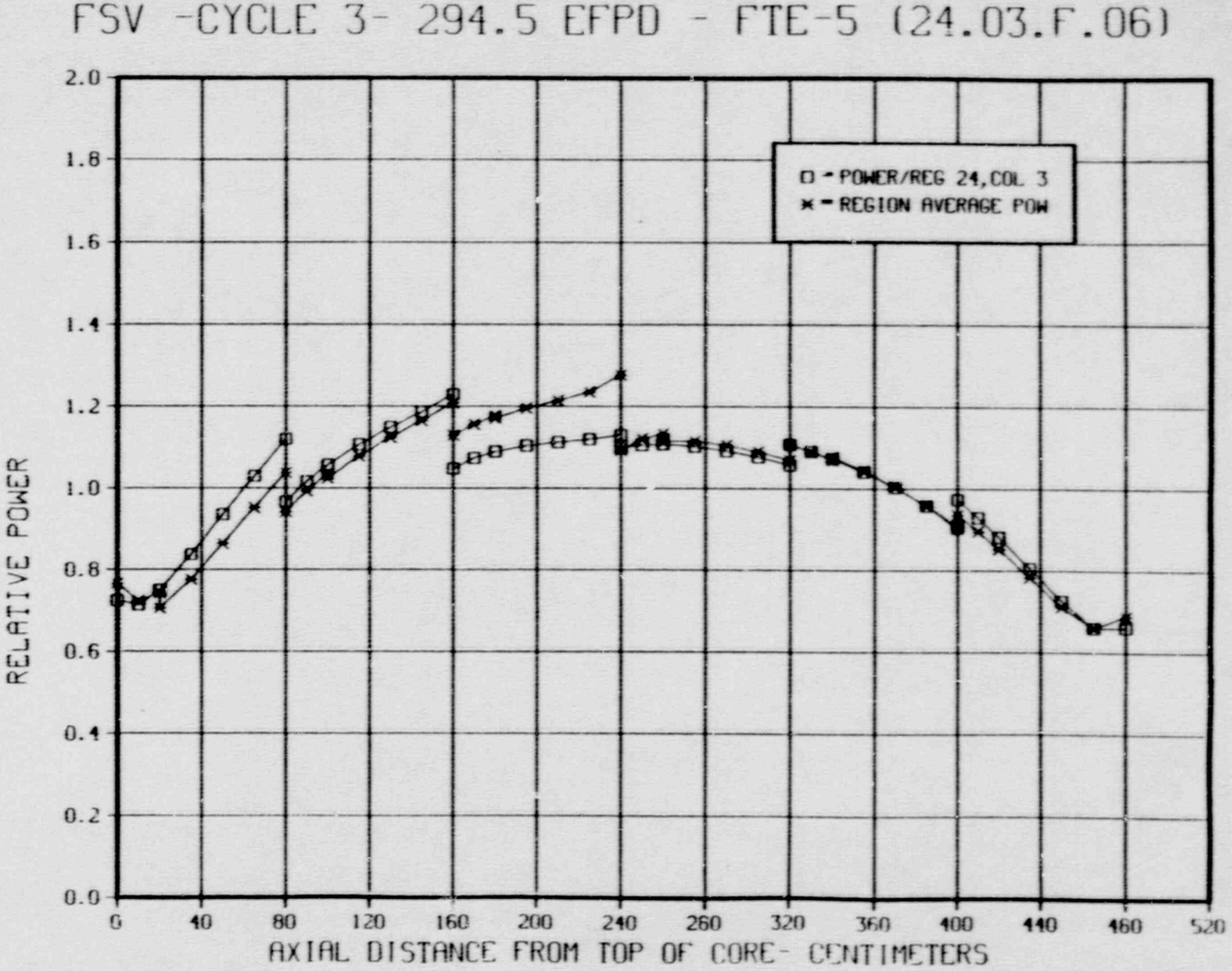
FSV -CYCLE 3- 294.5 EFPD - FTE-5 (24.03.F.06)
□ - POWER/REG 24,COL 3
* - REGION AVERAGE POW
RELATIVE POWER
AXIAL DISTANCE FROM TOP OF CORE- CENTIMETERS
0.0
0.2
0.4
0.6
0.8
1.0
1.2
1.4
1.6
1.8
2.0
0
40
80
120
160
200
240
280
320
360
400
440
480
520

Fig. 4-5

TABLE 4-6
HEAVY METAL CORE LOADING

	BOC1	EOC1	BOC2	EOC2	BOC3	EOC3
Th-232, kg	15,905	15,785	15,276	15,151	14,697	14,510
U-233*, kg	0	103	87	168	139	232
U-235, kg	721	552	655	498	624	410
Uranium, kg	774	740	829	785	881	804
Plutonium**, kg	0	1.0	0.9	1.8	1.6	3.2
U-233 enrichment, %	0	14.0	10.5	21.5	15.8	28.9
U-235 enrichment, %	93.1	74.5	79.0	63.5	70.9	51.0
Net enrichment***, %	93.1	88.5	89.5	84.9	86.6	79.9

*Assumes full decay of Pa-233.
**Assumes full decay of Np-239.
***(Mass of U-235 + U-233)/mass of uranium.

TABLE 4-7
FRACTIONAL FISSIONS

	BOC1	EOC1	BOC2	EOC2	BOC3	EOC3
U-233	0.0	0.196	0.150	0.303	0.225	0.408
U-235	1.0	0.798	0.846	0.688	0.769	0.580
Pu-239	0.0	0.004	0.002	0.006	0.003	0.007

TABLE 4-8
SEGMENT BURNUP

Fuel Segment	Burnup (MWd/tonne)*		
	EOC1	EOC2	EOC3
1	6,352	--	--
2	6,496	13,000	--
3	8,398	17,312	29,400
4	10,750	21,134	36,267
5	10,396	21,024	34,383
6	10,622	20,975	36,417
7	--	12,345	30,308
8	--	--	20,895
Core Ave.**	8,836	17,632	31,279

*Megawatt days per initial metric tonne of thorium plus uranium.

**Assumes all segments are equal volume.

The reactivity discrepancy is monitored throughout the cycle (see Refs. 1 to 8). Calculations are done using the 7-group GAUGE model and during cycles 1 and 2 these calculations, in general, overpredicted the core reactivity by approximately 0.0065 $\Delta k \pm 0.0015\ \Delta k$. This 0.0065 Δk is the calculational reactivity bias. Then, the reactivity discrepancy is defined as the difference between the calculated k_{eff} and 1.0065, i.e., the deviation from the calculational bias.

Figure 4-6 shows the calculated k_{eff} minus the measured k_{eff} (i.e., 1.00) as a function of EFPDs for cycle 3. These results indicate that the prediction of the initial cold criticality was as expected (i.e., confirming that the "as-built" segment 8 fuel and LBP loadings were very close to the design values). However, with burnup, the variation of the cold critical predictions has a larger spread than in previous cycles, especially near the middle of the cycle. The cause for the larger spread in the predictions can be at least partially explained by larger uncertainties in the measured data. A review (by PSC and GA) of the measured data recorded for the cold critical conditions throughout cycle 3 indicated that there were significantly larger uncertainties in the measured data recorded near the middle of the cycle than at the beginning and end of the cycle. Additionally, the uncertainties in the measured data (in particular, uncertainties in the recorded core inlet and outlet temperatures) for the middle of cycle cases were sufficient to cause the observed deviations from the bias. Therefore, it is concluded that the calculational reactivity bias of 0.0065 Δk is still valid for cold criticalities.

The data in Fig. 4-6 show that the calculational bias for the hot operating conditions is increased to approximately 0.0090 Δk with an uncertainty, except in a few cases, of approximately 0.0015 Δk.

The increase in reactivity discrepancy (i.e., the deviation from the calculational bias) at about 50 EFPDs was shown to be due to the inadvertent release of the reserve shutdown material into region 27, and the increase at about 140 EFPDs was due to an actual core power that was up to

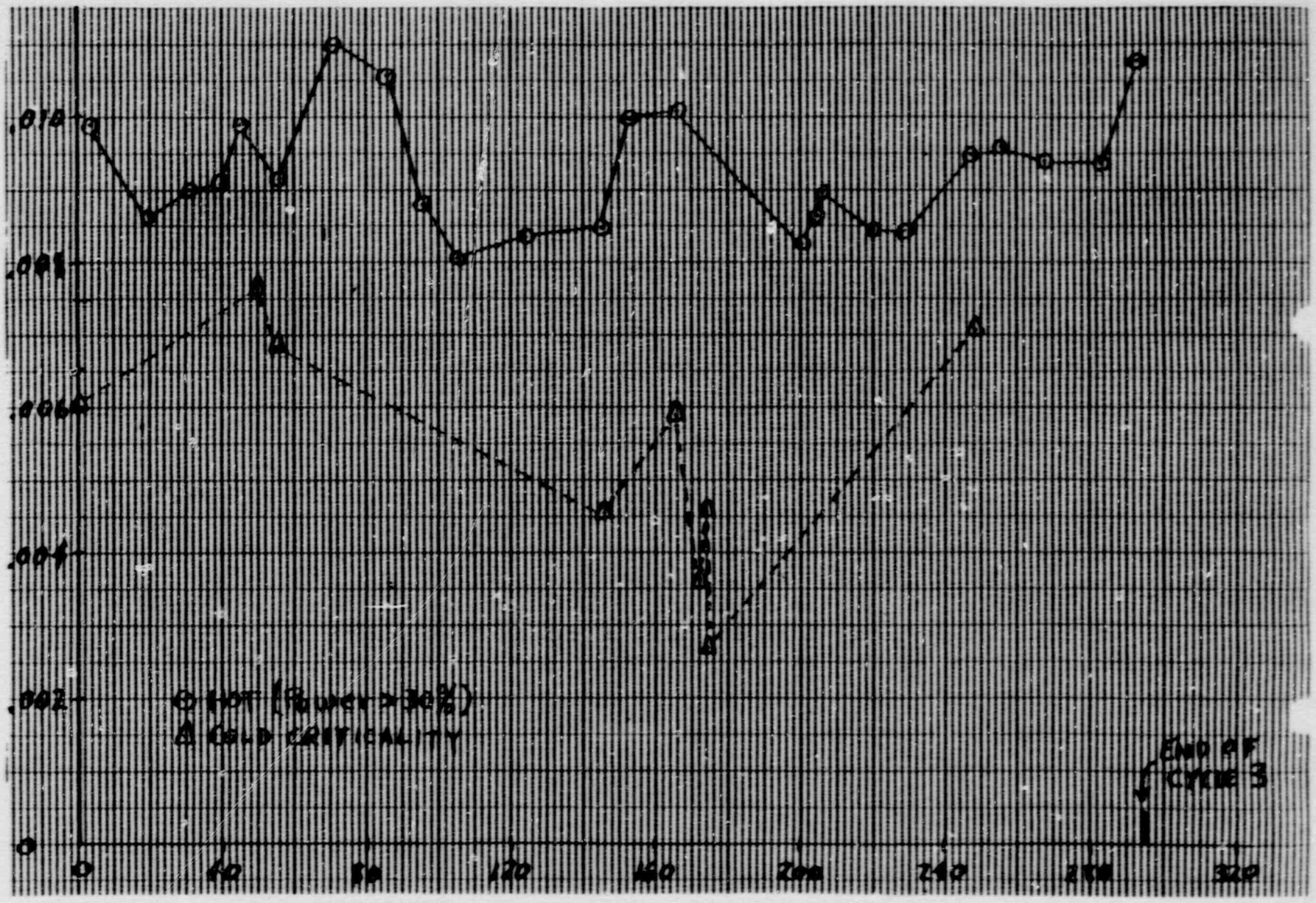

Fig. 4-6 CALCULATED MINUS MEASURED K_{eff} AS A FUNCTION OF CYCLE 3 BURNUP

10% higher than the official power level reported. At 200 EFPDs the decrease in reactivity discrepancy was the result of including the overburn in the calculation.

It is concluded that the cold reactivity bias for cycle 3 is unchanged from the previous value of 0.0065 $\Delta k \pm 0.0015\ \Delta k$, but the hot reactivity bias increased to approximately 0.0090 $\Delta k \pm 0.0015\ \Delta k$. This increase is due, in part, to uncertainties in core temperature. Since both the cold and hot reactivity bias remained relatively constant throughout cycle 3, the reactivity discrepancy remained small.

4.7. CONTROL ROD MANAGEMENT

The irradiation history of control rod pairs was calculated based on the flux distributions calculated with the GATT model (Section 4.5). The cumulative fast neutron fluence of the absorber clad (canister) is given in Table 4-9, the cumulative thermal neutron fluence of the clad is given in Table 4-10, and the burnup of absorber compacts is given in Table 4-11. The calculated results are in good agreement with the predictions based on the GAUGE model given in Ref. 24. Note that the irradiation history was compiled based on the assumption that individual rod pairs have remained in the same core region since the beginning of the initial cycle. It is known, however, that some rods have been interchanged within the core and some rods have been exchanged with spare rods. Therefore, until a clear record of all such rod exchanges is available, it is not possible to make realistic assumptions about individual rod history. However, at this stage of irradiation, parameters are so much lower than the limits that the exact knowledge of the exposure of each rod is not necessary.

TABLE 4-9
FAST NEUTRON EXPOSURE OF CLAD[1]
(TOTAL FOR 3 CYCLES)

CONTROL ROD SEGMENT[2]

Control Rod Pair	A	B	C	D	E	F	Avg[3]	Max[4]
1	0.00	0.00	5.27+18	2.46+20	9.20+20	1.49+21	4.43+20	1.49+21
2	0.00	0.00	0.00	0.00	0.00	3.00+20	5.00+19	3.00+20
3	0.00	0.00	0.00	0.00	2.13+18	2.83+20	4.75+19	2.83+20
4	0.00	0.00	0.00	0.00	0.00	2.86+20	4.77+19	2.86+20
5	0.00	0.00	0.00	0.00	1.73+18	3.03+20	5.08+19	3.03+20
6	0.00	0.00	0.00	0.00	0.00	2.97+20	4.95+19	2.97+20
7	0.00	0.00	0.00	0.00	2.81+18	3.07+20	5.16+19	3.07+20
8	2.83+20	3.87+20	3.96+20	3.24+20	2.40+20	3.56+20	3.31+20	3.96+20
9	4.62+20	6.09+20	6.22+20	5.39+20	4.63+20	5.36+20	5.38+20	6.22+20
10	1.97+20	3.02+20	4.12+20	4.25+20	4.08+20	5.17+20	3.77+20	5.17+20
11	6.43+20	8.98+20	9.48+20	8.49+20	8.93+20	9.29+20	8.60+20	9.48+20
12	3.21+20	4.26+20	4.32+20	3.55+20	2.67+20	3.71+20	3.62+20	4.32+20
13	4.22+20	5.56+20	5.83+20	4.92+20	4.19+20	4.70+20	4.90+20	5.83+20
14	1.69+20	2.61+20	3.54+20	3.82+20	3.67+20	4.99+20	3.39+20	4.99+20
15	6.23+20	8.68+20	9.34+20	8.42+20	8.84+20	9.06+20	8.43+20	9.34+20
16	3.11+20	4.24+20	4.40+20	3.56+20	2.66+20	3.74+20	3.62+20	4.40+20
17	5.19+20	6.91+20	7.02+20	5.56+20	4.72+20	5.11+20	5.75+20	7.02+20
18	1.57+20	2.44+20	3.37+20	3.55+20	3.44+20	4.51+20	3.15+20	4.51+20
19	6.55+20	9.09+20	9.53+20	8.54+20	8.95+20	9.30+20	8.66+20	9.53+20
20	7.15+19	1.02+20	1.08+20	8.59+19	7.47+19	2.05+20	1.08+20	2.05+20
21	1.92+19	2.53+19	3.39+19	5.88+19	1.07+20	4.32+20	1.13+20	4.32+20
22	1.60+20	2.28+20	2.46+20	2.01+20	1.74+20	3.12+20	2.20+20	3.12+20
23	2.82+18	4.19+18	4.28+18	3.01+18	1.98+18	1.60+20	2.93+19	1.60+20
24	2.86+19	4.44+19	5.83+19	6.65+19	8.43+19	3.34+20	1.03+20	3.34+20
25	0.00	0.00	0.00	0.00	0.00	2.37+20	3.95+19	2.37+20
26	7.83+19	1.12+20	1.19+20	9.59+19	8.46+19	2.06+20	1.16+20	2.06+20
27	1.65+19	2.10+19	3.00+19	5.82+19	9.50+19	3.91+20	1.02+20	3.91+20
28	1.34+20	1.92+20	2.10+20	1.75+20	1.54+20	3.26+20	1.98+20	3.26+20
29	2.83+18	4.20+18	4.28+18	3.01+18	1.98+18	1.48+20	2.74+19	1.48+20
30	3.24+19	4.99+19	6.46+19	7.27+19	9.17+19	3.38+20	1.08+20	3.38+20

TABLE 4-9 (Continued)

Control Rod Pair	A	B	C	D	E	F	Avg(3)	Max(4)
31	0.00	0.00	0.00	0.00	0.00	2.58+20	4.29+19	2.58+20
32	6.70+19	9.60+19	1.03+20	8.26+19	7.26+19	2.05+20	1.04+20	2.05+20
33	1.53+19	2.00+19	2.81+19	5.34+19	9.00+19	3.78+20	9.75+19	3.78+20
34	1.72+20	2.45+20	2.65+20	2.18+20	1.90+20	3.41+20	2.38+20	3.41+20
35	2.60+18	3.86+18	3.93+18	2.75+18	1.82+18	1.66+20	3.02+19	1.66+20
36	2.24+19	3.44+19	4.41+19	4.80+19	5.73+19	2.84+20	8.17+19	2.84+20
37	0.00	0.00	0.00	0.00	0.00	2.57+20	4.29+19	2.57+20

(1) Flux > 0.18 MeV (exposure in nvt).
(2) A + F - top segment to bottom segment.
(3) Average exposure of all 6 segments.
(4) Maximum segment exposure.

TABLE 4-10
THERMAL NEUTRON EXPOSURE OF CLAD[1]
(TOTAL FOR 3 CYCLES)

CONTROL ROD SEGMENT[2]

Control Rod Pair	A	B	C	D	E	F	Avg[3]	Max[4]
1	0.00	0.00	0.00	1.59+19	6.87+20	1.13+21	3.05+20	1.13+21
2	0.00	0.00	0.00	0.00	0.00	0.00	0.00	0.00
3	0.00	0.00	0.00	0.00	0.00	7.36+18	1.23+18	7.36+18
4	0.00	0.00	0.00	0.00	0.00	0.00	0.00	0.00
5	0.00	0.00	0.00	0.00	0.00	7.10+18	1.18+18	7.10+18
6	0.00	0.00	0.00	0.00	0.00	0.00	0.00	0.00
7	0.00	0.00	0.00	0.00	0.00	9.25+18	1.54+18	9.25+18
8	1.95+20	2.64+20	2.89+20	2.81+20	2.14+20	1.63+20	2.34+20	2.89+20
9	2.77+20	3.56+20	4.03+20	4.14+20	3.50+20	3.32+20	3.56+20	4.14+20
10	8.27+19	1.14+20	1.83+20	2.28+20	2.36+20	2.34+20	1.79+20	2.36+20
11	3.62+20	4.79+20	5.23+20	5.51+20	5.89+20	6.27+20	5.22+20	6.27+20
12	1.76+20	2.36+20	2.60+20	2.54+20	1.97+20	1.49+20	2.12+20	2.60+20
13	2.72+20	3.52+20	4.00+20	4.25+20	3.61+20	3.35+20	3.58+20	4.25+20
14	9.17+19	1.26+20	2.00+20	2.39+20	2.50+20	2.42+20	1.91+20	2.50+20
15	3.69+20	4.89+20	5.28+20	5.52+20	5.75+20	6.03+20	5.19+20	6.03+20
16	1.72+20	2.33+20	2.56+20	2.53+20	1.96+20	1.51+20	2.10+20	2.56+20
17	2.55+20	3.31+20	3.81+20	4.23+20	3.53+20	3.33+20	3.46+20	4.23+20
18	9.38+19	1.32+20	2.10+20	2.54+20	2.63+20	2.52+20	2.01+20	2.63+20
19	3.73+20	4.92+20	5.37+20	5.62+20	6.00+20	6.39+20	5.34+20	6.39+20
20	5.91+19	7.69+19	8.55+19	8.39+19	7.44+19	6.82+19	7.47+19	8.55+19
21	8.44+18	1.11+19	1.25+19	3.02+19	3.26+19	1.12+20	3.44+19	1.12+20
22	9.31+19	1.21+20	1.36+20	1.40+20	1.18+20	1.04+20	1.19+20	1.40+20
23	2.02+18	3.03+18	3.11+18	2.75+18	1.98+18	1.28+18	2.36+18	3.11+18
24	1.49+19	1.93+19	2.82+19	3.43+19	4.65+19	6.49+19	3.47+19	6.49+19
25	0.00	0.00	0.00	0.00	0.00	0.00	0.00	0.00
26	6.55+19	8.53+19	9.56+19	9.46+19	8.52+19	7.93+19	8.42+19	9.56+19
27	9.81+18	1.25+19	1.38+19	3.69+19	4.12+19	1.25+20	3.99+19	1.25+20
28	1.05+20	1.37+20	1.55+20	1.62+20	1.39+20	1.25+20	1.37+20	1.62+20
29	2.14+18	3.20+18	3.29+18	2.91+18	2.09+18	1.35+18	2.50+18	3.29+18
30	1.69+19	2.20+19	3.14+19	3.80+19	5.10+19	7.17+19	3.85+19	7.17+19

TABLE 4-10 (Continued)

Control Rod Pair	A	B	C	D	E	F	Avg[3]	Max[4]
31	0.00	0.00	0.00	0.00	0.00	0.00	0.00	0.00
32	6.84+19	8.90+19	1.00+20	9.88+19	8.83+19	8.17+19	8.77+19	1.00+20
33	9.37+18	1.20+19	1.32+19	3.54+19	3.93+19	1.47+20	4.27+19	1.47+20
34	8.94+19	1.16+20	1.31+20	1.35+20	1.15+20	1.02+20	1.15+20	1.35+20
35	2.29+18	3.42+18	3.52+18	3.10+18	2.23+18	1.44+18	2.67+18	3.52+18
36	1.71+19	2.23+19	3.16+19	3.78+19	4.76+19	6.32+19	3.66+19	6.32+19
37	0.00	0.00	0.00	0.00	0.00	0.00	0.00	0.00

(1) Flux < 2.38 eV (exposure in nvt).
(2) A + F - top segment to bottom segment.
(3) Average exposure of all 6 segments.
(4) Maximum segment exposure.

TABLE 4-11
CONTROL ROD BURNUP[1]
(TOTAL FOR 3 CYCLES)

CONTROL ROD SEGMENT[2]

Control Rod Pair	A	B	C	D	E	F	Avg[3]	Max[4]	Bottom[5] Compact
1	0.00	0.00	8.50-04	4.12-02	8.26-02	1.32-01	4.28-02	1.32-01	1.32-01
2	0.00	0.00	0.00	0.00	0.00	5.04-02	8.40-03	5.04-02	8.45-02
3	0.00	0.00	0.00	0.00	3.00-04	4.77-02	8.01-03	4.77-02	7.95-02
4	0.00	0.00	0.00	0.00	0.00	4.46-02	7.43-03	4.46-02	7.50-02
5	0.00	0.00	0.00	0.00	2.85-04	4.51-02	7.57-03	4.51-02	7.55-02
6	0.00	0.00	0.00	0.00	0.00	4.95-02	8.25-03	4.95-02	8.31-02
7	0.00	0.00	0.00	0.00	3.78-04	5.10-02	8.56-03	5.10-02	8.46-02
8	2.48-02	3.37-02	3.57-02	3.24-02	2.46-02	4.63-02	3.29-02	4.63-02	6.68-02
9	3.68-02	4.78-02	5.15-02	4.94-02	4.32-02	5.99-02	4.81-02	5.99-02	7.59-02
10	1.31-02	2.06-02	2.87-02	3.24-02	3.19-02	5.66-02	3.06-02	5.66-02	7.60-02
11	4.92-02	6.77-02	7.41-02	7.45-02	7.44-02	8.07-02	7.01-02	8.07-02	8.43-02
12	2.42-02	3.24-02	3.43-02	3.12-02	2.40-02	4.66-02	3.21-02	4.66-02	6.75-02
13	3.52-02	4.61-02	5.01-02	4.89-02	4.27-02	5.79-02	4.68-02	5.79-02	7.32-02
14	1.29-02	2.03-02	2.81-02	3.16-02	3.15-02	5.63-02	3.01-02	5.63-02	7.56-02
15	4.95-02	6.77-02	7.39-02	7.44-02	7.31-02	7.85-02	6.95-02	7.85-02	8.20-02
16	2.37-02	3.22-02	3.43-02	3.11-02	2.40-02	4.72-02	3.21-02	4.72-02	6.84-02
17	3.68-02	4.83-02	5.19-02	5.05-02	4.37-02	5.77-02	4.82-02	5.77-02	7.24-02
18	1.27-02	2.03-02	2.84-02	3.20-02	3.17-02	5.59-02	3.02-02	5.59-02	7.49-02
19	5.07-02	6.91-02	7.53-02	7.56-02	7.54-02	8.16-02	7.13-02	8.16-02	8.53-02
20	5.45-03	7.58-03	8.19-03	7.40-03	6.36-03	3.73-02	1.20-02	3.73-02	5.82-02
21	1.16-03	1.53-03	2.62-03	3.88-03	9.06-03	3.89-02	9.53-03	3.89-02	5.57-02
22	1.00-02	1.40-02	1.54-02	1.38-02	1.19-02	3.59-02	1.68-02	3.59-02	5.35-02
23	2.03-04	2.99-04	3.06-04	2.43-04	1.69-04	3.42-02	5.90-03	3.42-02	5.67-02
24	1.69-03	2.55-03	3.47-03	4.27-03	5.35-03	3.89-02	9.37-03	3.89-02	6.08-02
25	0.00	0.00	0.00	0.00	0.00	3.26-02	5.43-03	3.26-02	5.49-02
26	6.02-03	8.40-03	9.14-03	8.35-03	7.27-03	3.60-02	1.25-02	3.60-02	5.55-02
27	1.19-03	1.52-03	2.86-03	4.37-03	9.10-03	3.92-02	9.70-03	3.92-02	5.62-02
28	1.01-02	1.41-02	1.58-02	1.44-02	1.25-02	3.45-02	1.69-02	3.45-02	5.09-02
29	2.11-04	3.10-04	3.18-04	2.53-04	1.75-04	3.27-02	5.66-03	3.27-02	5.42-02
30	1.92-03	2.88-03	3.86-03	4.70-03	5.87-03	3.89-02	9.69-03	3.89-02	6.04-02

TABLE 4-11 (Continued)

Control Rod Pair	A	B	C	D	E	F	Avg[3]	Max[4]	Bottom[5] Compact
31	0.00	0.00	0.00	0.00	0.00	3.47-02	5.78-03	3.47-02	5.84-02
32	5.87-03	8.20-03	8.93-03	8.21-03	7.10-03	3.46-02	1.22-02	3.46-02	5.35-02
33	1.13-03	1.47-03	2.69-03	4.15-03	9.10-03	4.04-02	9.82-03	4.04-02	5.67-02
34	1.01-02	1.40-02	1.55-02	1.39-02	1.20-02	3.62-02	1.70-02	3.62-02	5.41-02
35	2.13-04	3.12-04	3.19-04	2.56-04	1.78-04	3.23-02	5.60-03	3.23-02	5.38-02
36	1.67-03	2.52-03	3.33-03	3.96-03	4.66-03	3.52-02	8.56-03	3.52-02	5.55-02
37	0.00	0.00	0.00	0.00	0.00	3.48-02	5.80-03	3.48-02	5.86-02

(1) Burnup in fraction of initial boron.
(2) A → F - top to bottom segment.
(3) Average burnup of all segments.
(4) Maximum segment burnup.
(5) Bottom boron compact of bottom segment.

5. THERMAL/FLOW PERFORMANCE

5.1. REGION PEAKING FACTOR

Throughout cycle 1, 2, and 3 operation, the distribution of power generation among the 37 refueling regions of the core was monitored. The power distribution is characterized by the region peaking factor (RPF), which is the ratio of the average power in a region to the core average power. The RPFs are monitored to demonstrate that the power distributions are within the limits stated in the bases of Technical Specification LCO 4.1.3.

Analyses of measured and computed RPF distributions during cycles 1, 2, and 3 have shown significant RPF discrepancies* (>10%) for the northwest (NW) boundary regions 20 and 32-37. The discrepancies in these regions are typically negative (indicating a measurement lower than the calculation) and increase with core pressure drop. Other regions exhibit smaller discrepancies and are essentially independent of core pressure drop. The major cause of the RPF discrepancies in the NW boundary regions is a transverse flow of relatively cool helium from the core-reflector interface along the region exit thermocouple sleeve (Type II flow). This flow passes over the region exit thermocouple assemblies of these regions and depresses the indicated region exit temperature. The driving potential for Type II

---

*The RPF discrepancy is defined as the percentage difference between the measured and calculated RPF, i.e.,

$$\text{RPF Discrepancy} = 100\left(\frac{\text{RPF}_{\text{meas.}} - \text{RPF}_{\text{calc.}}}{\text{RPF}_{\text{calc.}}}\right)$$

uniform fuel temperature. (See Ref. 3 for details of this calculational procedure.) This calculation was done for each control rod group, as the groups are withdrawn in sequence. These data were then interpolated to determine the RPF distribution for any specific operating control rod group configuration. This procedure was repeated throughout the cycle as required by SR 5.1.7.

- The measured RPF distribution, used in determining the RPF discrepancy distribution, was generated with the FSVCOR code (Ref. 29) using the calculated region exit temperature for regions 20 and 32-37 and the measured exit temperature for all other regions, as discussed in Ref. 28. This measured RPF distribution is then compared to the calculated distribution to determine the RPF discrepancy distribution. The calculated RPF distribution was generated with the 7-group GAUGE code, using fuel temperatures generated above with the FSVCOR code and atom densities from the most recent GAUGE fuel accountability calculations. Details of these calculational procedures are described in Refs. 28 and 60. This calculation is repeated as required by SR 5.1.7.

A typical measured and calculated RPF distribution and the RPF discrepancy distribution is shown in Fig. 5-1 for a power level of ~70% and a cycle 3 burnup of 264 EFPDs.

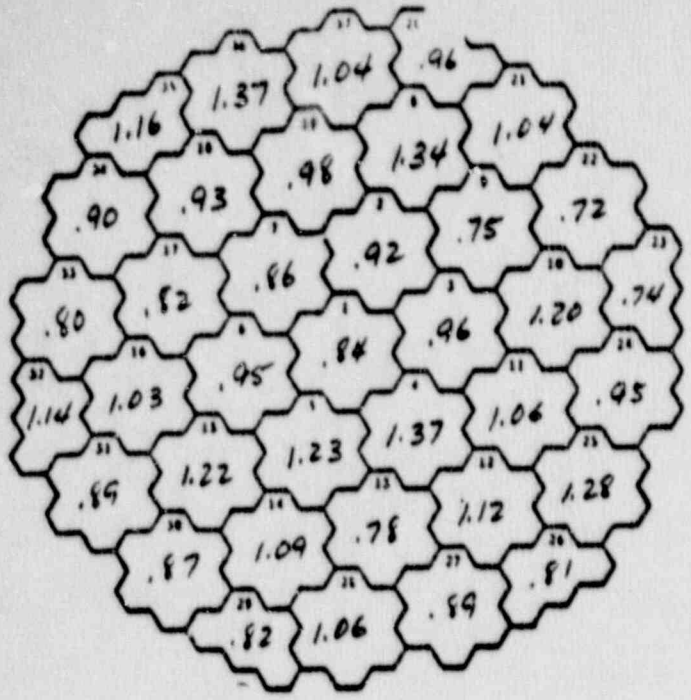

Measured RPF
Distribution
(December 16, 1983)

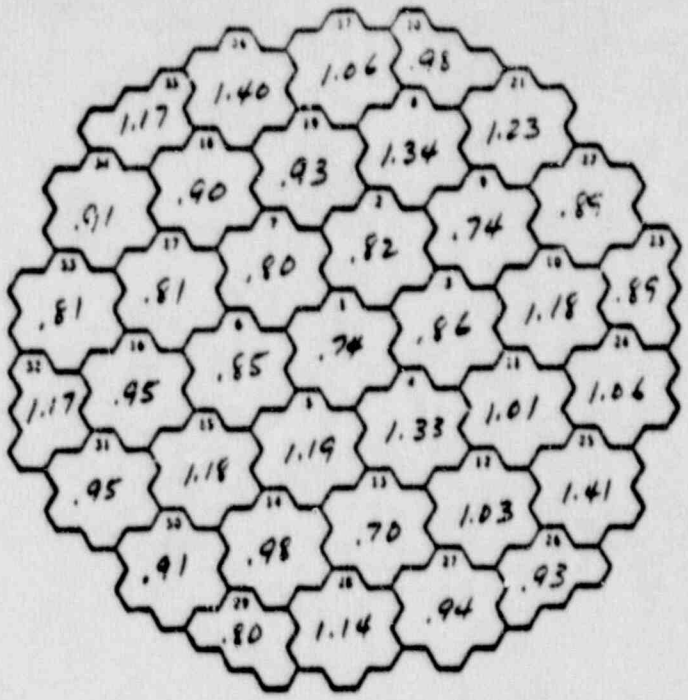

Calculated RPF
Distribution

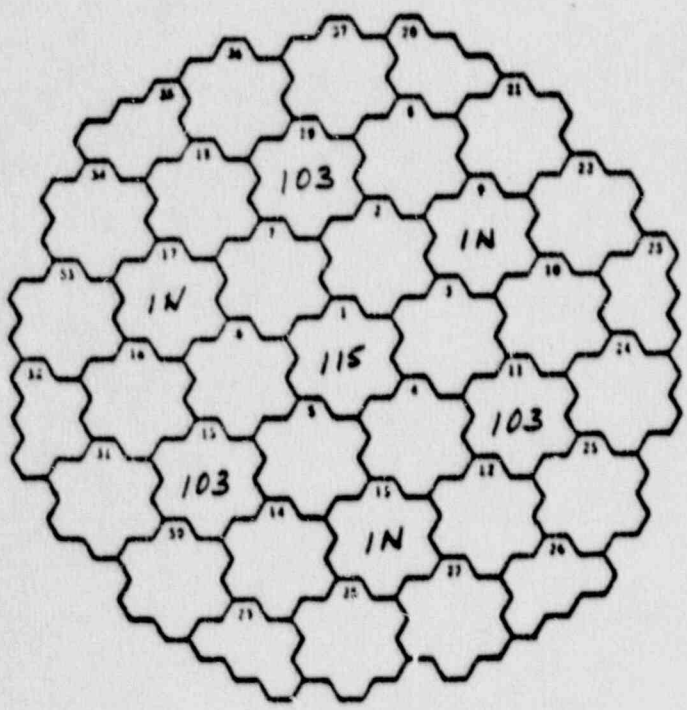

Control Rod
Positions (in.)

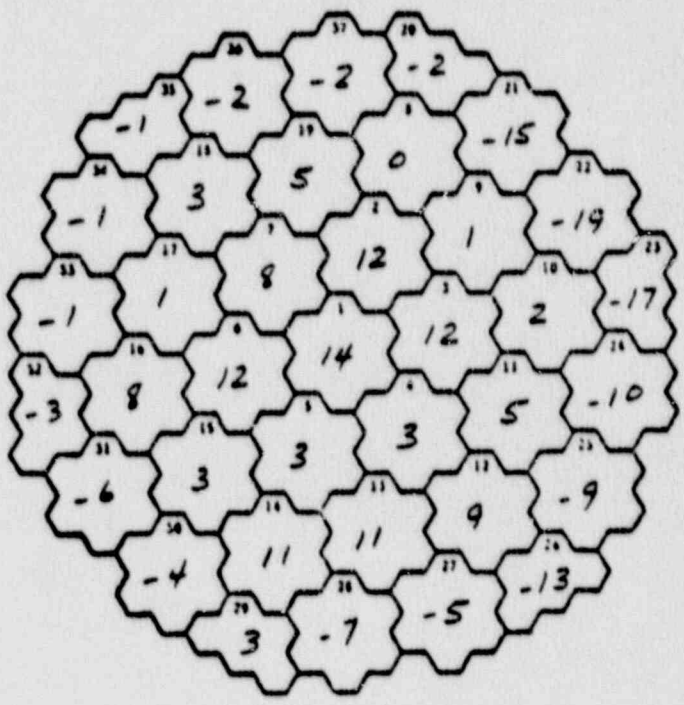

RPF Discrepancy
Distribution

Fig. 5-1 COMPARISON OF MEASURED AND CALCULATED RPF DISTRIBUTION

6. FUEL PERFORMANCE

Fuel performance calculations were performed to provide predictions of fission product activity using the SURVEY and TRAFIC computer codes (Refs. 62 and 63). Comparisons of measured and calculated fission product release have significant implication since they validate, either directly or indirectly, many of the methods currently used in FSV reload fuel segment design and core performance monitoring. These methods involve calculation of core power distributions, fuel temperature distributions, fuel particle failure, and fission product release. Cycles 1 and 2 were reanalyzed, along with cycle 3, since significant improvements have recently been made to the fuel failure models.

6.1. CALCULATIONAL METHODS

The fuel performance models defined in Refs. 62, 63, 65, 66, and 67 were used in these analyses. These models differ significantly from the ones (essentially the FDDM/B models) used in the previous cycle 1 and 2 analyses (Refs. 68 and 69). The main differences are discussed below.

- F_0 (the probability of an OPyC coating failure upon a SiC coating failure) is now explicitly modeled. It is given in FDDM/E as a function of burnup and temperature. This modeling of partially failed particles has a significant impact upon fission product release, since it allows for retention of fission gases for particles with failed SiC but intact OPyC coatings. In previous analyses, bounding values for F_0 ($F_0 = 0$ and $F_0 = 1$) had to be assumed.

- The model for fission gas release from as-manufactured heavy metal contamination was revised so that contamination fractions for thorium and uranium are now input, and temperature dependence of the release from contamination is now decoupled from the one for failed particles. The thorium and uranium contamination fractions used in this analysis were taken from QC records for various service-limit fuels and reload segments (Ref. 59).

- The model for fission gas release from failed fuel particles was completely revised in FDDM/E. Separate formulations were provided for hydrolyzed and unhydrolyzed fuel, also allowing for different temperature dependence of the release. The analysis was first performed by assuming that failed fuel particles were completely hydrolyzed as this corresponds to the standard design practice. However, since this assumption may be too conservative, the analysis was also performed for the unhydrolyzed condition.

- Fission product SiC corrosion was not considered in previous fuel performance analyses since this reaction has been assumed to be nonexistent in the FSV fuel. However, recent reexamination of the FSV fuel samples indicated some presence of this reaction (Ref 45). For this reason it was recommended, in Refs. 66 and 71, that this failure mode be included in FSV fuel performance analyses. This recommendation was followed in these analyses.

In order to predict nominal fuel particle failure, all the calculations were performed at 50% confidence level. The calculated fission gas release, based on the FDDM/E fuel performance models, substantially exceeded the measurements. A review of the FDDM/E fuel performance models indicated that there was excessive conservatism in the failure model for particles with missing buffer coatings. In the FDDM/E model the probability of failure for particles with missing buffers increased linearly

from zero at zero burnup to one at a relative burnup ($FIMA/FIMA_{max}$) of 0.2. In order to provide a more realistic appraisal of failure in fuel with missing or defective buffers, the FDDM/E model was revised in Ref. 71 for the FSV fuel. The revised model gives the failure probability as a function of the relative burnup, fuel temperature and kernel porosity; the physical assumption is that kernel porosity provides a limited reservoir for the storage of fission gases. As recommended in Ref. 71, a kernel porosity of 7% was used, and the analysis with the revised model was performed.

The metallic release calculations were performed for the key nuclides Sr-90, Cs-134, and Cs-137. Direct release calculations for Sr-90 and Cs-137 were done with the TRAFIC code. In the previous analysis (Ref. 69), which was based on the FDDM/B performance models, a constant transition concentration (from Henrian to Freundlich sorption isotherms) was used, while in this analysis, based on FDDM/E models, the transition concentration is a function of temperature. Also, the sorptivity of graphite for metals is now calculated as a function of fluence.

For Sr-90 and Cs-137, the contribution from precursor decay was determined by calculating the R/Bs for Kr-90 and Xe-137 from the predicted R/Bs for the reference isotopes Kr-85m and Xe-138.

6.2. RESULTS

6.2.1. Fuel and Graphite Temperatures

Figures 6-1 and 6-2 show the volume distributions of the peak and time averaged fuel temperature for segment 6, which is assumed to be a typical segment. The maximum and time-averaged fuel temperatures of 1262°C (2304°F) and 918°C (1684°F) were predicted. For the entire core the peak and time-averaged maximum fuel temperatures of 1440°C (2624°F) and 1128°C (2063°F) were predicted. These maximum temperatures were predicted to occur in segment 7, region 28, column 5, local point 5, which is in a

Peak Fuel C/L Temperature Distribution
Segment 6

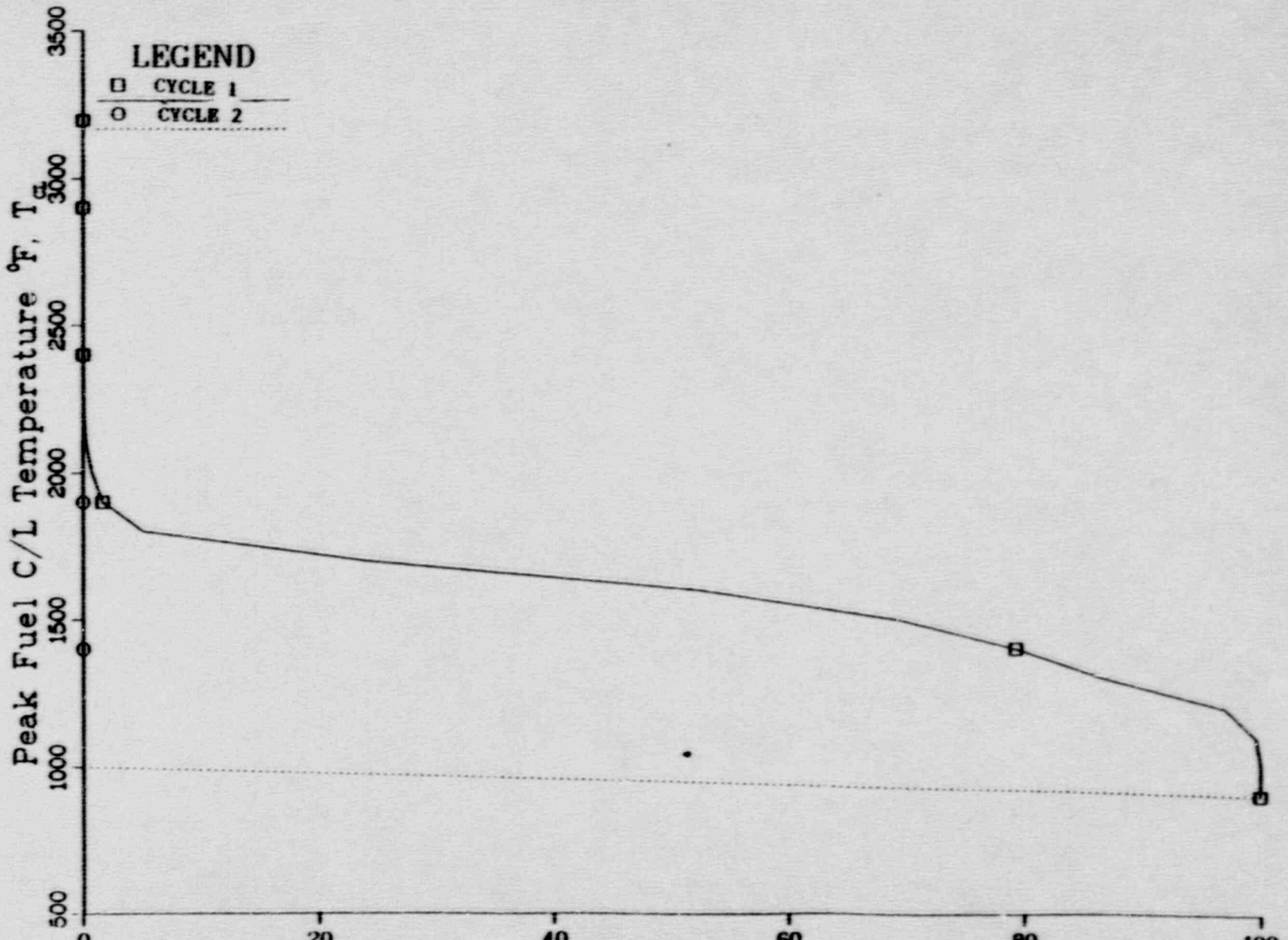

Fig. 6-1

Time Averaged Fuel C/L Temperature Distribution

Segment 6

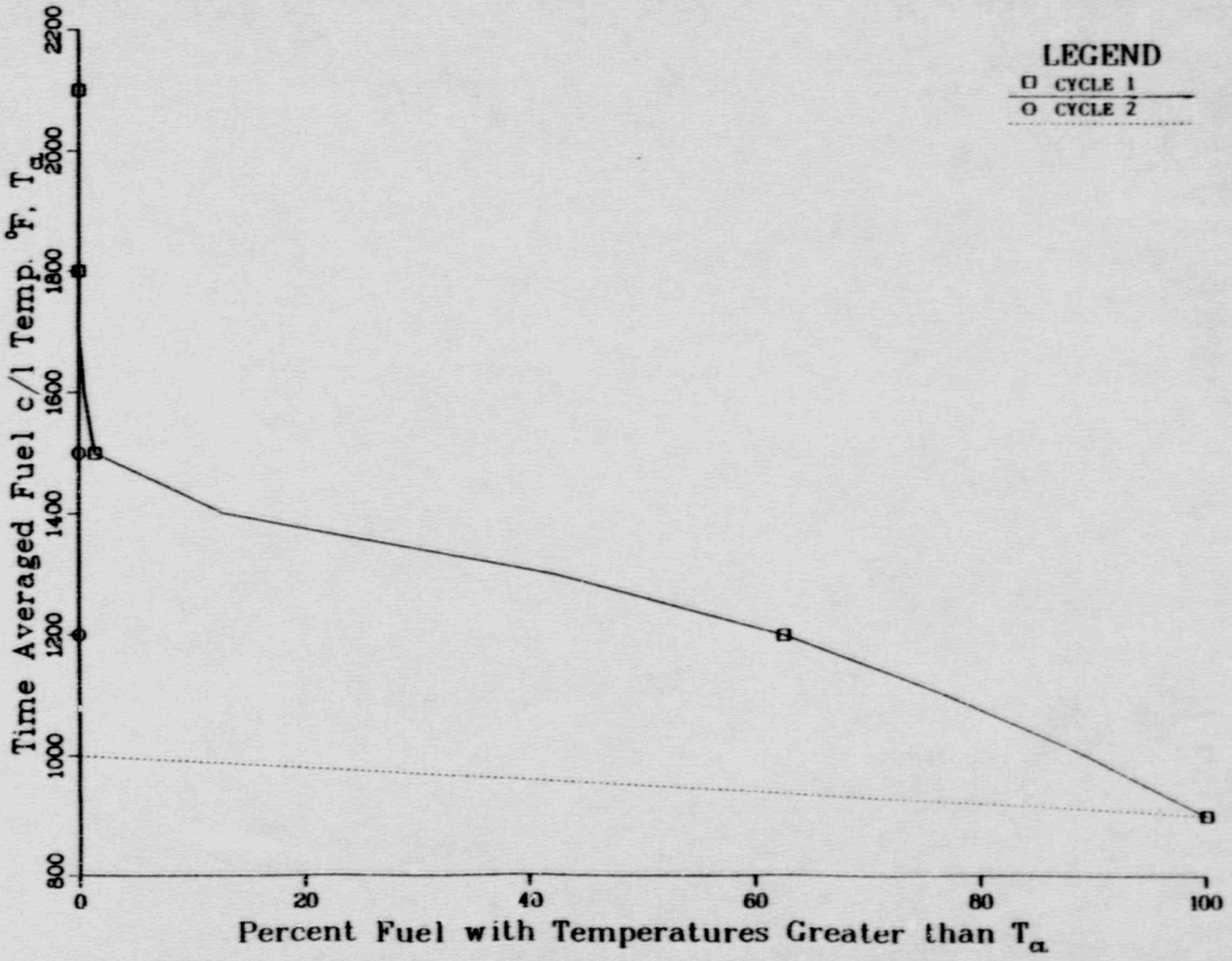

Fig. 6-2

thin-buffered column. Previous analyses of such partially buffered columns have indicated that the predicted intercolumn power tilts can be excessively conservative, resulting in large overpredictions of fuel temperatures, as was the case for the above point. Even though the above maximum temperature is considered excessive, it was not discarded from the analysis since it is a result of the current methodology of analyzing the partially buffered columns. The peak graphite temperature, predicted to occur at that location, was 1394°C (2542°F) and 1092°C (1998°F) on a time-average basis. These high graphite temperatures have a large impact on the predicted cesium release as discussed in Section 6.2.4.

6.2.2. Fuel Particle Failure

At the end of cycle 3 the maximum fissile and fertile burnups were calculated to be less than 15% and 2.5% FIMA, respectively. These values are lower than the design values of 20% and 7% FIMA for segments 1-6.

Fuel volume distribution of fast neutron fluence for segment 6 is shown in Fig. 6-3. The maximum fast fluence at the end of cycle 3 was less than 3.5×10^{21} n/cm^2, which is lower than the design value of 8×10^{21} n/cm^2 for segments 1-6.

Time histories of fuel particle failure by different mechanisms are shown in Figs. 6-4 and 6-5 for the fissile and fertile fuel. These failures are based on the revised manufacturing defects failure model. The maximum predicted fissile fuel particle failure from all mechanisms was 0.072% with 83% of the total failure from the manufacturing defects. For the fertile particle the maximum predicted failure from all mechanisms was 0.023% with 48% of the total failure from the SiC-fission product interaction. This failure is due to high fuel temperatures in some parts of the core and particularly in the buffered fuel blocks, which dominates the manufacturing defects failure as the latter is strongly burnup-dependent and burnup was rather low in the fertile fuel during the first three cycles. It should be noted that in the earlier analyses the SiC-fission

Fast Neutron Fluence Distribution by Year
Segment 6

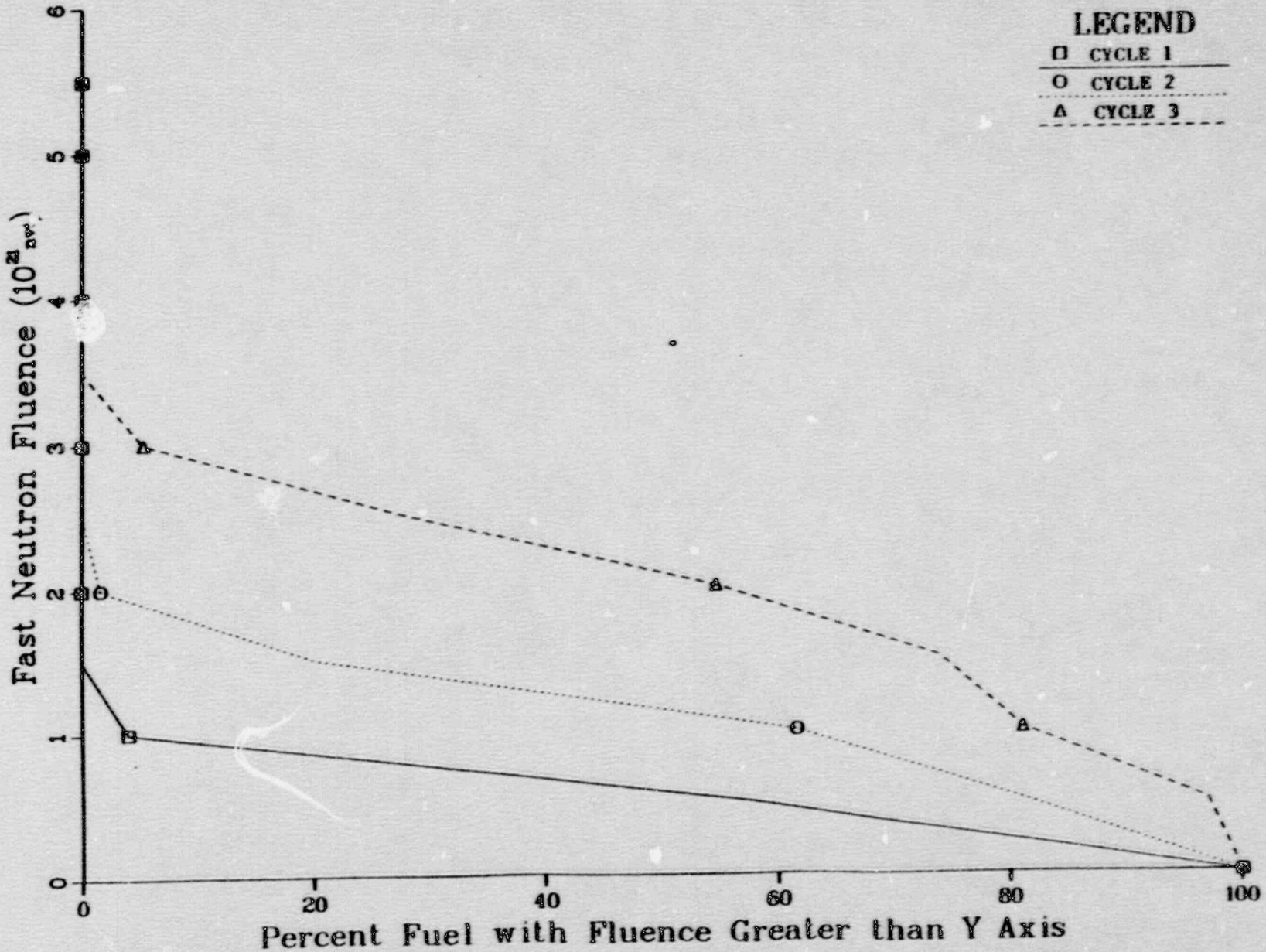

Fig. 6-3

Failed Particle Percentage by Failure Types
Particle 1, $(Th/U)C_2$
Core Average

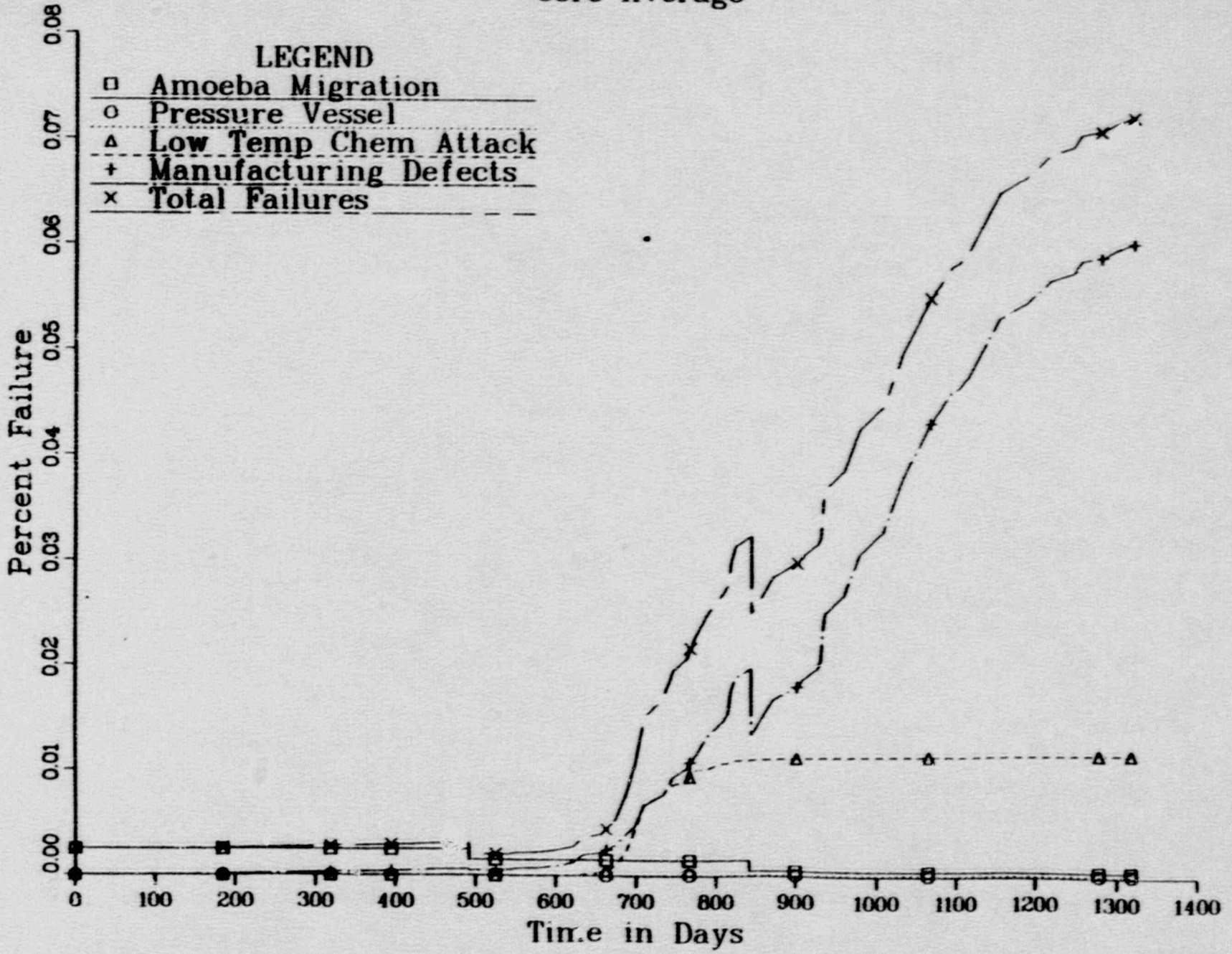

Fig. 6-4

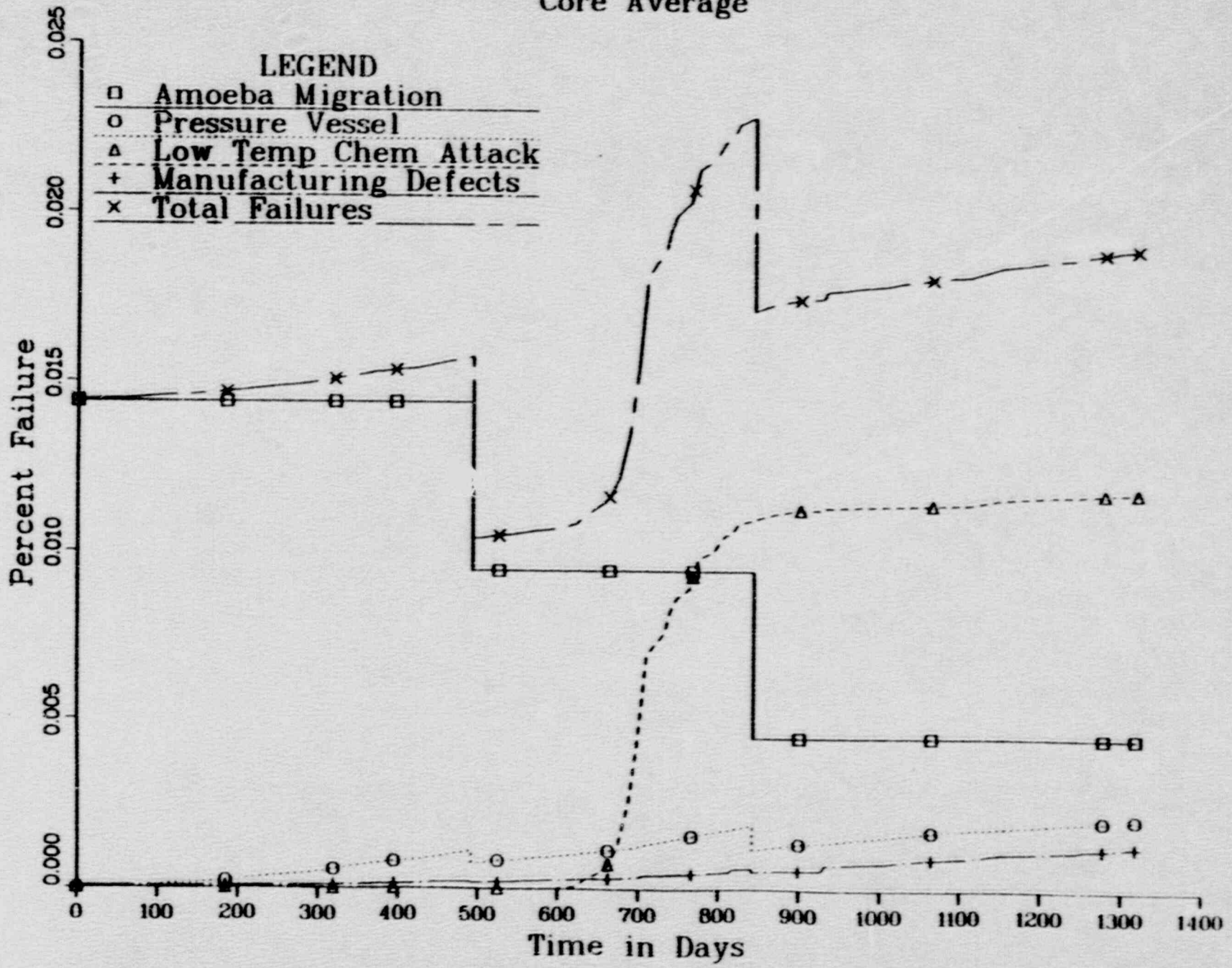
Failed Particle Percentage by Failure Types
Particle 2, ThC_2
Core Average
LEGEND
Amoeba Migration
Pressure Vessel
Low Temp Chem Attack
Manufacturing Defects
Total Failures
Percent Failure
0.000
0.005
0.010
0.015
0.020
0.025
0
100
200
300
400
500
600
700
800
900
1000
1100
1200
1300
1400
Time in Days

Fig. 6-5

product interaction was assumed to be nonexistent in the FSV fuel particles. The fissile particle failure, which is far more dominant than the fertile failure, is predicted to be rather low up to approximately the middle of cycle 2 as a result of the revised manufacturing defects model where, due to low burnup, the failure due to missing buffers is low. However, during the remainder of cycle 2, the burnup in most of the fissile fuel (in conjunction with fuel temperature) exceeds the threshold value beyond which a rapid increase in manufacturing defects failure is predicted according to the revised model for missing buffers.

6.2.3. Gaseous Fission Product Release

A comparison of the predicted and measured fission gas release for the key nuclide Kr-85m is shown in Figs. 6-6 and 6-7. Figure 6-6 shows the predictions based on both the original FDDM/E and the revised manufacturing defects models with the assumption of completely hydrolyzed failed fuel. A comparison of the predicted release rate-to-birth rate ratio (R/B) with measured data (Ref. 32) indicates that the R/B based on the original FDDM/E manufacturing defects model exceeds the data early in cycle 1 due to large predicted manufacturing defects failure, due primarily to missing buffer layers. As discussed earlier, this large overprediction prompted the revision of the manufacturing defects model. With the revised model, there is good agreement between the predicted R/B and measured data up to approximately the middle of cycle 2 when the predictions start to exceed the data, resulting in a factor of five overprediction at the end of cycle 3. This overprediction can be the result of either or both of the following two effects: (1) in spite of the revision in the particle failure model, the failure fraction is still overpredicted at moderate and large burnup, and (2) the in-pile effect of fuel hydrolysis is less than observed in tests; although hydrolysis has been shown to dramatically increase the R/B from failed carbide fuel in laboratory tests and in short-term TRIGA tests (Ref. 72), irradiation and thermally induced sintering mitigates substantially the long-term in-reactor consequences. In order to assess these two effects, the analysis was performed for

COMPARISION OF MEASURED Kr-85m RELEASE DATA AND PREDICTIONS FOR FORT ST. VRAIN

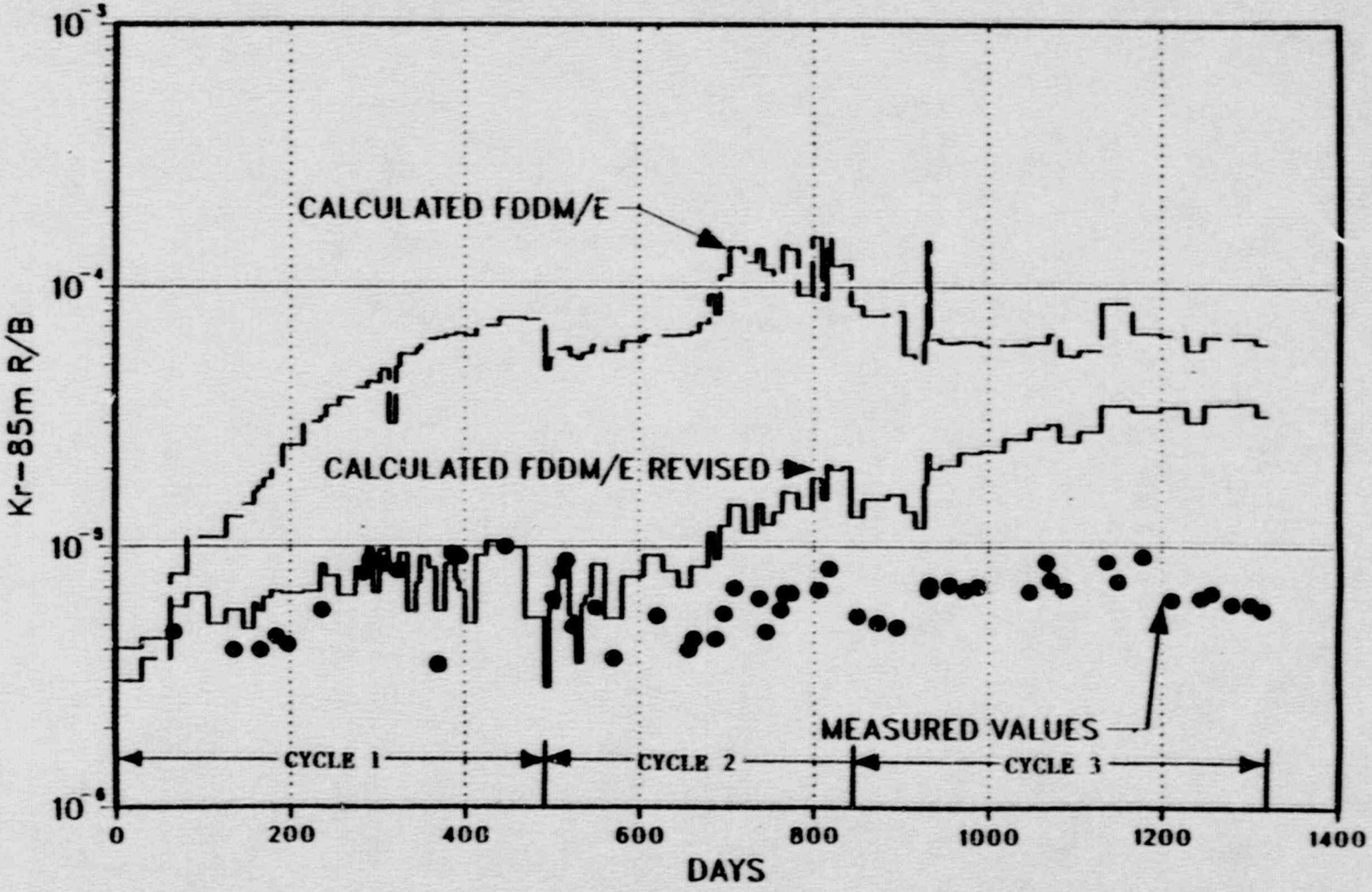

Fig. 6-6

COMPARISION OF MEASURED Kr-85m RELEASE DATA AND PREDICTIONS FOR FORT ST. VRAIN

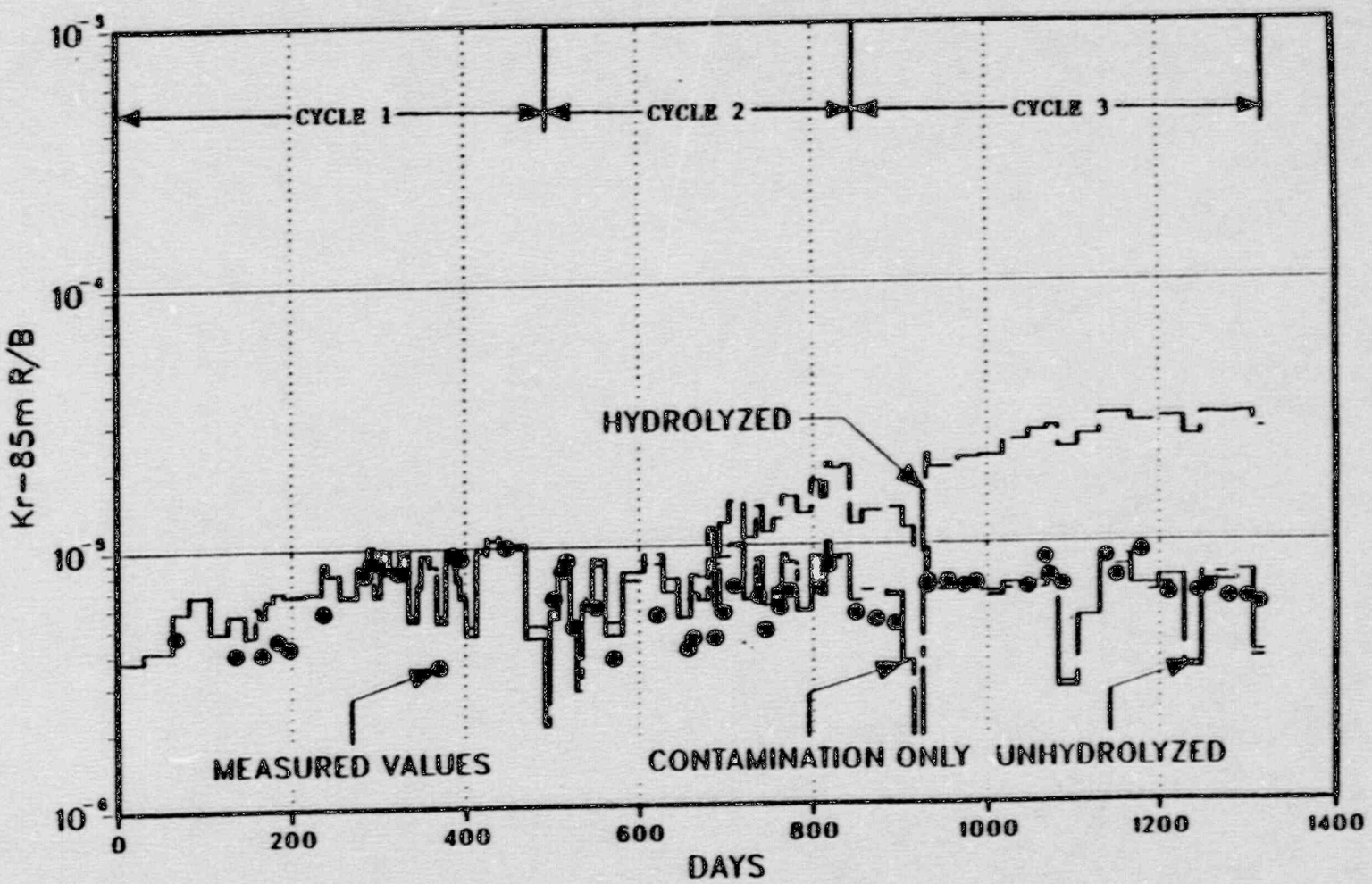

Fig. 6-7

(1) the case with no particle failure where the only contribution to fission gas release is due to as-manufactured heavy metal contamination, and (2) the unhydrolyzed condition. The results, shown in Fig. 6-7, indicate that excellent agreement with data was obtained throughout the first three cycles for both cases. Consequently, the cause of the overprediction remains ambiguous. Long-term in-pile hydrolysis tests with carbide fuel would be required to resolve this issue.

6.2.4. Metallic Fission Product Release

The results of the metallic fission product release analysis for Sr-90, Cs-134, and Cs-137 are shown in Tables 6-1, 6-2, and 6-3, respectively. Also shown are the plateout probe data (Ref. 33) and the results of the previous analysis for the first two cycles (Ref. 69).

A comparison of the results of this analysis with data indicates that, in general, the agreement is reasonably good. For Sr-90 the predicted release of 0.37 Ci compares well with the measured values of 0.2 to 0.66 Ci. The direct release of Sr-90 as calculated with the TRAFIC computer code was negligible, and the only contribution was from the precursor (Kr-90) decay. A comparison of the Sr-90 predicted release from this and the previous analysis indicates that EOC1 and EOC2 values predicted in this analysis are lower due to the lower predicted fuel particle failures resulting from the use of the new failure models. For Cs-134 and Cs-137 the agreement with data is not as good as for Sr-90. For Cs-134 the analysis overpredicted the data by a factor of 6.8. For Cs-137 the total predicted release was 5.0 Ci while the measured values ranged from 1.3 to 1.9 Ci. This agreement could be improved by making a correction for the excessive release predicted for the maximum temperature point in the core. As discussed in Section 6.2.1, even though the temperatures predicted for this maximum temperature point (the buffered portion of the region 28, column 5, axial block 6) are considered to be in excess of actual temperatures, they were not removed from the analysis. Due to excessively high predicted graphite temperatures, the graphite attenuation

TABLE 6-1
Sr-90 RELEASE (Ci)

	EOC1		EOC2		Plateout Probe Removal Time		EOC3
	This Analysis	Previous Analysis	This Analysis	Previous Analysis	This Analysis	Data	This Analysis
Direct release (from TRAFIC code)	0	0	0	0	0		0
Precursor (Kr-90) Decay contribution	0.14	0.59	0.32	1.44	0.37		0.60
Total	0.14	0.59	0.32	1.44	0.37	0.66*	0.60

*"Total circuit" value from Table 4-11 of Ref. 33; the "on dust" value of 0.2 Ci was reported.

TABLE 6-2
Cs-134 RELEASE (Ci)

	EOC1 Analysis	EOC2 Analysis	Plateout Probe Removal Time Analysis	Plateout Probe Removal Time Data	EOC3 Analysis
Release	0.01	2.2	3.4	0.5*	8.0

*From Table 4-11 of Ref. 33.

TABLE 6-3
CS-137 RELEASE (Ci)

	EOC1		EOC2		Plateout Probe Removal Time		EOC3
	This Analysis	Previous Analysis	This Analysis	Previous Analysis	This Analysis	Data	This Analysis
Direct release (from TRAFIC code)	0.05	35.0	9.9	212.9	11.8		19.0
Direct release (after correcting for mixed isotope and mixed species)	0.02	12.1	3.4	73.5	4.1		6.6
Precursor (Xe-137) decay contribution	0.33	0.4	0.8	1.1	0.9		1.5
Total	0.35	12.5	4.2	74.6	5.0	1.3*	8.1

*"Total circuit" value from Table 4-11 of Ref. 33; the "on dust" value of 1.9 Ci was reported.

of the cesium release is substantially reduced at this point resulting in excessive predicted release. The release at this point is predicted to amount to over 90% of the direct release from the entire core. If this release is replaced with the release from a similar partially buffered element where the predicted fuel and graphite temperatures are considered reasonable, the total direct release would be substantially reduced. Thus for Cs-137, the corrected total release would be 1.1 Ci which is in excellent agreement with the data. A similar improvement can be obtained for the Cs-134 predicted release. A comparison of the predicted Cs-134 release in this and the previous analysis indicates that the release predicted in this analysis is considerably lower due to the lower predicted fuel particles failures as a result of the use of the new fuel failure models.

6.3. CONCLUSIONS

The results of this analysis, based on the revised FDDM/E performance models indicate that excellent agreement was obtained between the predicted and measured fission gas release for the key isotope Kr-85m during the first cycle and approximately half of the second cycle. After this time the predictions exceed the data, and at the end of cycle 3 the data is overpredicted by a factor of five. This overprediction can be the result of either or both of the following two effects: (1) in spite of the revision in the fuel particle failure model, the failure fraction is still overpredicted at moderate and large burnups, and (2) the in-pile effect of hydrolysis is less than observed in laboratory and TRIGA tests. In order to assess these two effects further analysis was performed for (1) the case with no particle failure where the only contribution to fission gas release is due to as-manufactured heavy metal contamination, and (2) the unhydrolyzed condition. The results indicate that either hypothesis is plausible. For the release of the fission metals Sr-90, Cs-134, and Cs-137, reasonably good agreement was obtained between the predictions and data from the plateout probe. The agreement was excellent for Sr-90.

However, the predictions for cesium exceeded the data. For Cs-134 the analysis overpredicted the data by a factor of 6.8. For Cs-137 the predicted release was 5.0 Ci while the measured values ranged from 1.3 to 1.9 Ci. This agreement could be improved by making a correction for the excessive release predicted for the maximum temperature point in the core. This point is located in a partially buffered fuel element where fuel and graphite temperatures were overpredicted due to excessively high predicted intercolumn tilts. Due to these high fuel and graphite temperatures, the cesium release at the maximum temperature point is predicted to be over 90% of the total release from the entire core. If this release is replaced with the release from a similar partially buffered fuel element, where the predicted fuel and graphite temperatures are considered reasonable, the predicted Cs-137 release would be 1.1 Ci which is in excellent agreement with the data. A similar improvement can be made for the Cs-134 predicted release.

A comparison of the gaseous and metallic fission product release predicted in this and the previous analysis for the first two cycles indicates that the release predicted in this analysis is considerably lower. This is due mainly to lower fuel particle failure fractions predicted as a result of the use of the new fuel particle models. New models for the fission gas and metal release have also been used in this analysis.

Based on the results of this analysis, the following conclusions can be made regarding the fuel performance methodology.

- The manufacturing defects fuel particle failure model should be further examined regarding the failure of particles with missing buffer coatings at moderate and high burnup to determine if there is still excessive conservatism in the model.

- In order to provide a definitive answer to the perennial question of the effect of fuel hydrolysis on fission gas release during reactor operation, in-pile hydrolysis data is needed. Planned hydrolysis tests (Ref. 70) may provide some of these answers, although these tests are for a different fuel (UCO).

7. SPECIAL TESTS AND SURVEILLANCES

Throughout each cycle, special tests and surveillances are performed to provide additional data for core performance evaluation. Results of cycle 2 and 3 tests and surveillances are summarized below (cycle 2 results are those results which were not available for inclusion in the cycle 2 performance report).

7.1. CHEMISTRY SURVEILLANCE

Chemistry surveillance tests were performed throughout cycle 3 operation. Details of these test results are given in Refs. 30 through 32 and brief summaries of these results are given in the following sections.

7.1.1. Coolant Impurities

Surveillance data showed that at steady state 70% power operation the coolant impurities were low, totaling approximately 2 to 3 ppm CO + CO_2 + H_2O throughout the cycle. These results are similar to those data obtained in previous cycles.

7.1.2. Noble Gas Release/Birth (R/B)

The circulating noble gas activity was low with Kr-85m R/B at 6 to 7 x 10^{-6} throughout the cycle (at approximately 70% power) and virtually identical to previous cycles. This is significant in that it shows that fuel failure remains undetectable.

7.1.3. Tritium Concentrations

Primary coolant tritium concentrations during 1982 and 1983 were extremely low, in the 10^{-6} to 10^{-5} $\mu Ci/cm^3$ range which is below the expected concentration of $>3 \times 10^{-5}$ $\mu Ci/cm^3$. It was suspected, therefore, that the tritium monitor and/or the procedures were faulty (i.e., giving erroneously low results). Accordingly, tests at GA on a mock-up of the FSV tritium monitoring system were conducted.

Results of these tests show that the monitor concept installed at FSV is basically sound and capable of producing repeated tritium values which differ by no more than ±20%. Some refinements in procedure were required to obtain this reproducibility, in particular: (1) using long purge times before and between samples, (2) ensuring that the CuO bed is functioning, and (3) using a slightly higher CuO bed temperature.

The main conclusion of the tritium analysis is that the FSV data are correct. The explanation for the low tritium concentration throughout the cycle is that tritium is continuously being chemisorbed by the 1.2 million pounds of graphite in the core and reflector. This acts as a form of constant purification for hydrogen species, including H_2 and HT.

7.1.4. Iodine Monitor

Analysis of an iodine monitor test showed that a small amount of primary He contamination in the cold trap could account for the apparent high iodine concentrations, (relative to the plateout probe results). The contamination could explain the results, depending on when the contamination occurred, i.e., at the start or end of the test. Further tests were performed near the end of cycle 3 in which special precautions were taken to exclude primary coolant contamination from the gamma counting trap. This test showed that the apparent circulating iodine concentrations were ≤10% of that found earlier, suggesting that the early iodine monitor

results were erroneous (too high) due to contamination with primary loop helium.

7.1.5. Plateout on Circulator

The gamma and beta scan of circulator C-2101, removed at the end of cycle 2, showed low total activities permitting virtual hands-on maintenance. Much of the activity was due to activation products that apparently are transported in the circuit on dust particles. The concentration of these radioactive particles appeared to be constant in cycles 1 and 2. Rather vigorous wiping of the surface, however, could effect a removal portion of only 12%. Iodine and Cs plateout on the circulator was lower in cycle 2 than in cycle 1.

7.1.6. Gamma Activity of PGX Surveillance Samples

The gamma activity of the PGX surveillance samples (located in the lower reflector during cycle 2) was low, with activation products dominating the total radioactivity. Only 0.013 μCi of Cs-137 was found on the 23 g sample. This equates to approximately 50 μCi Cs-137 plateout per lower reflector element per fuel cycle.

7.1.7. Gamma Scanning of Circulator

The circulator C-2104 was removed to GA for refurbishment and repair after operating for three cycles. The inlet duct was analyzed for radioactive plateout, and showed that the concentrations of radionuclides were roughly equal to those found on circulator C-2101 after the first two cycles of operation. All of the circulator analyses to date show low levels of plateout, in general, ranging in the 1 to 1000 nanocuries per cm^2.

7.2. PLATEOUT PROBE

The plateout probe is a device that samples the hot primary coolant gas for condensible fission products. It allows the amount of circulating and condensed key fission products in the circuit to be calculated. Technical Specification LCO 4.2.8 limits the concentrations of I-131 and Sr-90, and the probe is intended to be the primary means of demonstrating compliance with LCO 4.2.8.

Radiochemical analysis of the plateout probe showed that the radioactive contamination in the primary circuit was remarkably low, with activation product concentrations much greater than that of fission products. The analysis demonstrates that the concentrations of the key fission products I-131 and Sr-90 are far below the limits allowed by LCO 4.2.8. This conclusion is reached even though the probe may not have quantitatively sampled iodine. Other available data on iodine behavior, including the iodine monitor and grab sample xenon R/B measurements can be used at present to show compliance with the iodine specification

Another important finding is that, to date, little or no barium, cesium, or strontium was directly released from the core. Rather, these volatile metals were released only via their gaseous precursors xenon and krypton. Once in the primary circuit, a large fraction of these metals apparently affix to small dust or aerosol particles and are thereby transported around the circuit. In addition, the concentrations of Ba-140 and Sr-90 show that the R/B of short half-life xenon and krypton isotopes can be accurately estimated by straight-line extrapolation of the R/B versus half-life ($t^{1/2}$) curve. Finally, the concentration of H_2S in the helium coolant is apparently below that required for deleterious sulphidation corrosion.

Details of the plateout probe radiochemical analyses are reported in Ref. 33.

7.3. CORE SUPPORT BLOCK OXIDATION

Core support block (CSB) oxidation is periodically monitored to determine the effect of graphite burnoff on the stresses in the CSB. The stresses considered in the analysis are due to the weight of the core, the differential pressure across the core, and the vertical acceleration loads resulting from an operational basis earthquake. CSB graphite burnoff is permitted until the stresses developed in the CSB graphite reach one-third the ultimate tensile strength of PGX graphite. At the end of the design exposure time, the stresses in the CSB will be approximately one-third of the ultimate tensile strength and the life of the block will have been consumed.

Previous oxidation studies of the 37 CSBs were evaluated for cycle 1 and 2 operation (Refs. 34 and 35). Region 27 was found to have the largest burnoff in each cycle. The maximum CSB life consumed after cycle 2 was 12.1%, which is well below the allowed service life. This study was then extended through December 1982, i.e., through the middle of cycle 3. Burnoff accumulated during the new period was calculated and added to previous burnoff profiles. However, the northwest boundary regions of the core were reanalyzed from the beginning of cycle 1 in order to correct the previous burnoff calculations for the effect of region exit temperature measurement errors (see Section 5).

Burnoff profiles for all 210 CSB coolant channels were predicted using the CSBBO-3 code (Ref. 36) and data from the data logger (DL) history tapes. Results of these analyses show that the column that experienced the most burnoff was in region 27 and this column had used 21.9% of its useful life at the middle of cycle 3 (MOC3). Details of these analyses are reported in Ref. 37.

These studies were then extended to the end of cycle 3 by estimating the oxidation using parametric rate curves derived for region 27, i.e., the region which experienced the most oxidation since the beginning of cycle 1

(Ref. 38). These results show that the cumulative oxidation for region 27 (the worst case location) had consumed approximately 28% of the useful life of the CSB at the end of cycle 3.

Approximately 40% of the burnoff for region 27 occurred at helium gas temperatures above 1400°F and moisture levels between 1 to 5 ppm. Also, the rate of burnoff during cycle 3 increased over past cycles. This is probably due to increased plant operation at high reactor power, and therefore, high gas temperatures.

Based on the average CSB oxidation rate from beginning of life through the end of cycle 3, the worst case CSB has approximately 22 years of remaining life. Since the CSBs are 8 years old, the 30-year CSB lifetime estimate remains valid.

7.4. PGX GRAPHITE SURVEILLANCE

A PGX graphite surveillance test element, inserted into the bottom reflector (in column 7 of region 25) during the first refueling, was removed at the end of cycle 2. Post-irradiation examination (PIE) of this element provided data on the oxidation of PGX graphite. Comparison of the measured oxidation to that predicted for the surveillance specimens then provides a basis for assessing the oxidation of the core support blocks. The surveillance specimens were exposed to reactor conditions similar to that experienced by the PGX graphite core support blocks.

The modified CSBBO-3 computer code (Ref. 39) was used to predict the oxidation in the PGX surveillance specimen based upon actual reactor performance data. The predicted oxidation of the PGX specimens is reported in Ref. 40. Predictions of PGX oxidation were based on a PGX oxidation rate which is 1000 times the H-451 graphite oxidation rate. Since only one PGX oxidation rate was assumed, the predicted oxidation varied only with temperature and moisture level.

The PIE of the surveillance specimens was performed according to specifications given in Ref. 41.

The results of the PIE of the surveillance samples and the comparison with predictions are given in Ref. 42. These results show that the PGX surveillance specimens exhibited significantly less oxidation than predicted. Overall oxidized weight loss averaged only 20% of the predicted values. Actual penetration depth of oxidation into the specimens was only about 50% of the predictions and the level of burnoff in the oxidized volumes was considerably lower than predicted. In all cases, the CSBBO-3 code predicted higher levels of oxidation and more severe oxidation profiles than observed in the surveillance specimens.

7.5. FUEL TEST ELEMENTS (FTEs)

During the loading of segment 7 (reload 1), eight test elements, FTE-1 through FTE-8, were loaded into layer six of regions 25, 22, 30, 27, 24, 10, 5, and 5, respectively.

These FTEs were manufactured from near-isotropic H-451 graphite instead of the needle-coke H-327 graphite used in the reference elements. This results in structurally stronger fuel elements with better heat transfer and dimensional change characteristics than those of the reference elements.

Reference fresh and recycle fuel for large HTGRs, as well as improved fuel contemplated for use in future FSV reload segments, was included in the FTEs. Improvements in the fuel include (1) ThO_2 fertile kernels, (2) HEU UC_2 and weak acid resin (WAR) fissile kernels, (3) cure-in-place fuel rod process, (4) a small number of fertile particles with BISO coatings, and (5) a small number of fuel rods containing LEU (Th,U) O_2 TRISO medium enriched uranium (MEU) fuel (19.5% enriched).

Details of these eight FTEs are given in Ref. 10.

The FTEs have a very small effect on the operation of the core under all conditions. The eight FTEs represent only a small percentage of the core (0.54%) and only six of the elements contain new fuel types, which represents only 0.40% of the total fuel. It was shown in Section 4.5.6 that these FTEs have an insignificant effect on the axial power distribution.

FTE-2 was removed from core region 22 at the end of cycle 3. An extensive post-irradiation examination (PIE) program was planned for this FTE (Amendment 2 of Ref. 10). However, with the exception of the graphite block metrology, this PIE program has not yet been performed. A reduced PIE program of FTE-2 fuel samples is now planned (funded by PSC). The results of the metrology examination indicate that FTE-2 underwent very little dimensional change as a result of irradiation. The visual examination provided observable and concrete evidence of the H-451 graphite structural integrity and performance. There were small scratches but no significant structural damage. Details of the FTE-2 examinations are reported in Ref. 51.

7.6. POST-IRRADIATION EXAMINATION OF FUEL AND REFLECTOR ELEMENTS

7.6.1. Segment 2 Elements

Fifty-four fuel and reflector elements from core segment 2, removed from the core during the second refueling, underwent nondestructive metrological and visual inspections in April 1982 in the hot service facilities at the reactor site. These inspections were part of the FSV Fuel Surveillance Program sponsored by the Department of Energy (DOE). The results of these inspections are reported in Ref. 43.

---

*Manufacturer's serial number.

During these inspections, two of the standard fuel elements, serial numbers (S/N) 1-2415* and 1-0172*, were discovered to have similarly aligned hairline cracks extending the entire axial length in the face adjacent to the large single dowel. The cracked web in fuel element 1-2415 was discovered during the on-site surveillance, whereas the crack in element 1-0172 was discovered via viewing video tapes and photographs from the surveillance and was later confirmed by visual examination performed in the GA hot cell (Ref. 44). Preirradiation inspection reports indicated that neither element was cracked prior to insertion into the core, and there was no record of any damage during handling. In addition, the fact that the cracks were colinear suggests that they developed during irradiation.

Both elements were manufactured from graphite grade H-327 and contained fuel rods consisting of $(Th,U)C_2$ TRISO fissile particles and ThC_2 TRISO fertile particles bonded together by a carbonaceous matrix. The nominal preirradiation dimensions of the fuel rods were 12.5 mm (0.49 in.) in diameter and 49.3 mm (1.94 in.) in length.

Both elements were irradiated in core refueling region 8, column 5. Element 1-2415 was located in axial layer 6 (active core layer 3) and element 1-0172 was located in axial layer 7 (active core layer 4). These elements, placed in the core in January 1974, were irradiated during cycles 1 and 2. During this time the average core burnup was 363 EFPDs.

Element 1-2415 was selected for destructive post-irradiation examination (PIE) because it exhibited the larger crack and experienced larger fast fluence and metrological changes than element 1-0172. The purpose of the destructive examination was to provide experimental data on the irradiated element, to verify its performance, and to acquire in-pile performance data. Tensile strength, thermal expansivity, and thermal diffusivity samples were taken from the irradiated graphite block. The fuel rod-graphite interaction was determined by measuring fuel stack pushout force. Gamma scans of a central fuel stack in each face were taken

so that power and burnup could be characterized. These data were analyzed and made available for other scoping analyses that were done to develop possible scenarios leading to the cracked web. A section of graphite from the emptied element was cleaned to do a qualitative study on the feasibility of cleaning spent graphite blocks for burial as low level waste. The results of the destructive examination of fuel element 1-2415 are reported in Ref. 45.

Extensive analytical investigations were made to evaluate the consequences of the cracked elements (Refs. 46, 47, and 48). The consequences of hypothetical fuel element damage causing coolant flow obstruction were reviewed with the NRC in response to questions raised in 1978 concerning core temperature fluctuations. The discussions also included the potential for misalignment of fuel elements in the event of dowel failure and the resulting effect on insertability of control rods and reserve shutdown balls.

A conservative assessment of the consequences of fuel element damage in terms of fuel particle failure, fission product release, and reactivity control was performed. This assessment is applicable in that it envelopes the consequences in the unlikely event that limited cracks of the type discovered were to propagate through a block.

Based on the above assessment and the NRC licensing review, it was concluded that there was no safety or operational limitation on continued reactor operation and/or fuel handling (Ref. 49).

7.6.2. Segment 3 Elements

Sixty-two fuel and reflector elements from core segment 3 were nondestructively examined in the FSV hot service facility (HSF) during June 1984. These examinations were performed as part of the DOE-sponsored surveillance program. The time- and volume-averaged graphite irradiation temperatures and volume-averaged fast neutron fluences for the elements

ranged from approximately 380°C to 670°C and from 0.96 to 2.82 x 10^{25} n/m^2, respectively. The examinations were intended to verify the structural integrity and dimensional stability of the elements and to obtain dimensional change data and gamma dose rates to verify HTGR design code calculations.

The axial and radial dimensions of nearly all the inspected H-327 graphite fuel elements shrank as a result of irradiation, but the dimensional changes were relatively small. The maximum element-average axial ($\Delta Z/Z$) and radial ($\Delta X/X$) strains were -0.73% and -0.57%, respectively. The maximum bow was 0.69 mm. The examined reflector elements underwent very little dimensional expansion (less than ±0.48 mm). The measured strains in segment 3 elements were reasonably close to or greater than the calculated dimensional changes. The measured bow was consistently higher than the calculated bow.

The visual examinations of the elements showed the elements to be in good condition. No cracks were observed. There was little evidence of graphite oxidation. The evidence of mechanical interactions (rub marks) was no more severe than in the two previous surveillances which suggested that the core movement was very minimal or had stopped. Minor dowel pin and dowel socket damage was observed on two elements, but the damaged areas did not affect the handling, storage, or the performance of the elements. A few chips, nicks, and other handling scratches were noted, but these blemishes did not affect the performance of the core components.

Strain calculations were performed with the HTGR code SURVEY/STRESS (Ref. 50) and the results compared with measured strains. The results of the comparison showed the calculated strains to be underpredicted in almost every case. The differences between the calculated and measured axial strains were, however, small, i.e., ≤0.4%.

Details of these segment 3 elements examinations are reported in Ref. 51.

7.7. GAMMA SCANNING OF FUEL ELEMENTS

The gamma scan robot was used to measure fission product isotopic distributions in fuel elements removed from the core at the end of cycle 3. Fourteen regular fuel elements and 3 control rod elements were gamma scanned to measure axial and radial profiles of selected fission products.

Cesium-137 activity profiles were in excellent agreement with calculated time-averaged power profiles. Similarly, Zr-95 activity profiles agreed with end-of-life power factors. Calculated and measured profiles agree statistically if a ±5% error in the calculated value is assumed.

Absolute Cs-137 activity was used to measure fuel element burnup (FIMA). The measured burnup in 12 of the 14 regular fuel elements agreed with the calculated burnup. In the two regular elements and the three control elements which did not agree, the measured burnup was significantly larger than the calculated value. Although the reasons are unclear, it appears that the measured value is in error since there is no reason for the particular elements to have a higher burnup than the other elements in the region.

These data are described in detail in Ref. 73.

7.8. SCRATCHER PLENUM ELEMENTS

In 1979, as part of the fluctuation investigation, a pair of special metal plenum elements were installed on adjacent columns of regions 18 and 3[illegible] the active core. One of these two elements was equipped with a "[illegible]" and one with a "stylus." The stylus was designed to reach [illegible] gap between the two regions and bear upon the surface of the [illegible]ad so that any relative motion between the two refueling regions would [illegible] recorded by scratching a pattern on the pad. (See Ref. 9 for a detailed description of the scratcher plenum elements.)

These special elements were removed during the third refueling. A visual examination of the scratch pad revealed a tear-shaped area of matte appearance caused by relative motion between the stylus and pad. This area was about 0.25 in. long and 0.06 in. wide at its maximum. Relative motion of the order of 0.25 in. is consistent with the relative motion between regions postulated to explain fluctuations (Ref. 52). The scratched pattern on the scratch pad constitutes the only direct measurement of relative motion between components of the core (i.e., adjacent columns and/or refueling regions). A video tape recording of the scratched appearance was made as part of the metrology examination.

7.9. TEMPERATURE FLUCTUATIONS

7.9.1. Background

During the initial rise-to-power program in October 1977, at ~60% power, temperature fluctuations were observed in the primary coolant circuit at individual core region outlets and at the steam generator module inlets. This, in turn, led to fluctuations in the main steam and reheat steam temperatures.

Fluctuations were observed during cycle 1 operation under a variety of core conditions at power levels from ~30% to ~70%. The effects of the fluctuations were observed in the nuclear channel signals, the region exit helium temperatures, and the steam generator module helium inlet temperatures. Data obtained during both planned fluctuation testing and fluctuations which occurred as a result of plant upsets or spontaneous events which occurred during normal power operation led to the identification of core pressure drop as an important operating parameter relative to the fluctuation threshold.* It was demonstrated that maintaining a low core

*The threshold line was defined as that line above which fluctuations had been initiated and below which fluctuations had not been initiated.

pressure drop obtained by opening the variable orifice valves) raised the threshold of fluctuations to at least 70% thermal power.

During the course of the cycle 1 investigation of the fluctuations there were many postulated theories for explaining the observed behavior. The most likely explanation of the temperature and neutron flux fluctuations was small movements of reactor components, such as fuel elements, reflector elements, and/or the core support floor. These small movements change the distribution of the gaps between the columns of graphite blocks which, in turn, cause changes in the bypass flow distribution in these gaps. This motion is most likely induced by pressure gradients in the gaps and thermal gradients in the core components causing component deformation and bowing. The movements are sustained by the feedback coupling of these two phenomena. Details of these cycle 1 tests and analyses are given in Ref. 53.

During the first refueling in early 1979 a comprehensive in-core inspection program indicated that no damage to the core components had occurred as a result of the fluctuations.

Cycle 2 operation began in May 1979 and the fluctuation testing program was continued. Fluctuations were again initiated at power levels from approximately 40% to 70%. Data from these tests demonstrated that while the fluctuations observed during cycle 2 were somewhat more regular and widespread throughout the core, they were basically the same phenomenon as experienced during cycle 1. The cycle 2 fluctuations indicated a similar dependence on core pressure drop to that of cycle 1, but the fluctuations occurred below the cycle 1 threshold. Details of the cycle 2 fluctuation testing and analyses, before installation of the region constraint devices (RCDs), are given in Ref. 52.

In October 1979 the plant was shut down and region constraint devices (RCDs) were installed as a means of eliminating the temperature fluctuations. These RCDs provide inter-region keying and, therefore, preclude the accumulation of large gaps. (See Ref. 9 for a description of the RCDs.)

In late 1980 tests were conducted to evaluate the effect of RCD installation on the fluctuation threshold. No fluctuations were detected, throughout these tests, at power levels up to approximately 70% and at core pressure drops up to approximately 4.2 psi, even though most of the testing was performed at conditions above the previously established fluctuation threshold line. However, during a power increase to approximately 59%, a resistance* of approximately 56 and a core pressure drop of approximately 3.4 psi, a redistribution in region exit temperatures was observed. In general, this redistribution resulted in the interior region exit temperatures increasing more than expected and the boundary region exit temperatures either not increasing as much as expected, or decreasing. Evidence of the temperature redistribution was also observed in the gap thermocouple (T/C) and instrumented control rod drive (ICRD) data, and in the nuclear detector response. This temperature redistribution was shown to be repeatable and in each case the temperatures returned to their expected values as the core power and pressure drop were reduced.

Analyses of these data indicated that the observed region exit temperature redistributions were the result of a redistribution of gaps (i.e., small block displacement). These displacements were similar in nature to the initial motion which occurred during fluctuations but the displacements showed no cyclic behavior.

---

*Resistance (R) = 2×10^{13} $(\Delta p P)/(T m^{1.85})$

where Δp = measured core pressure drop (psid)

P = PCRV pressure (psia)

T = average circulator inlet temperature (°R)

m = total circulator flow rate (lbm/h)

As a result of the fluctuation testing after installation of the RCDs, the Nuclear Regulatory Commission (NRC) issued a release to test above 70% power. These tests were performed in early 1981, during cycle 2 operation, at power levels up to approximately 90%, using the procedures of RT-500K* (Ref. 26). Basically, this test procedure specified 3% power increases (at -3%/min) from 40% to 100% power. Throughout the testing periods, special restrictions on the region exit temperatures were specified. In addition to the temperature limits of Technical Specification LCO 4.1.7, RT-500K required (1) a margin on the allowable region exit temperature mismatch**, (2) regions with temperature measurement errors be operated by comparison region, and (3) adjusted margins for operation after a temperature redistribution. Details of RT-500K and of these region exit temperature restrictions are discussed in Ref. 27.

Temperature redistributions again were observed during these tests, but no temperature fluctuations were evident.

7.9.2. Cycle 3 Testing

Cycle 3 operation began in July 1981 and RT-500K was again performed in late 1981. During these tests, no fluctuations were detected at power levels up to 100% of rated power but, again, regio.. exit temperature redistributions were observed. Details of the testing and analyses for cycles 2 and 3, after installation of the RCDs, are given in Refs. 27 and 54.

---

*RT-500 was originally performed in November 1978, during cycle 1 operation, as a part of the fluctuation test program. It has undergone numerous revisions as a result of test experience and for compatibility with cycle 2 operation.

**Temperature mismatch is defined as the deviation of the region exit temperature from the core average exit temperature.

Evaluations of the region exit temperature redistribution data indicated that these events involved no unreviewed safety questions. As a result of these tests, a method was developed for operating the core which accounts for region exit temperature measurement discrepancies both before and after a redistribution. Under this operating procedure, the seven northwest (NW) boundary regions which are susceptible to exit temperature measurement errors, i.e., regions 20 and 32 through 37, are operated by comparison regions in a manner similar to that employed in the test procedure. For the other 30 regions in the core, indicated changes in the region exit temperature which occur during a temperature redistribution are assumed to be correct. These temperature changes can be accommodated and corrected as desired by routine orifice valve adjustments. In support of this operating procedure, revisions to the Technical Specifications were developed (see Section 5.1 and Ref. 28). These revised Technical Specifications (LCO 4.1.7) were approved by the NRC in September 1982. After that time, the core was operated per these revised procedures.

Cycle 3 fluctuation testing demonstrated that RCDs were successful in preventing fluctuations at power levels up to 100% and at core pressure drops up to 5.0 psid.

7.10. RADIATION EXPOSURE HISTORY

The radiation exposure history for FSV is compared to that from light-water reactors (LWRs) in Table 7-1. The LWR data were obtained from Refs. 55, 56, and 57. These data show that the FSV radiation exposure per megawatt year has never exceeded 10% of the average of all United States LWRs.

TABLE 7-1
COMPARISON OF RADIATION EXPOSURE AT COMMERCIAL POWER REACTORS

	1978	1979	1980	1981	1982	1983
Average Collective Doses Per Reactor						
FSV HTGR	0.9	3.0	1.3	0.5	0.4	0.95
All U.S. LWRs	497.	597.	791.	773.	705.	753.
All U.S. PWRs	429.	516.	578.	652.	57[illegible]	592.
All U.S. BWRs	604.	733.	1136.	980.	940.	1056.
Average Gross Electric Generation Per Reactor (MW-Years)						
FSV HTGR	76.	28.	83.	94.	73.	94.
All U.S. LWRs	494.	447.	429.	449.	443.	
All U.S. PWRs	509.	434.	435.	467.	578.	
All U.S. BWRs	471.	467.	418.	419.	410.	
Average Man-Rem Per MW-Yr						
FSV HTGR	0.012	0.11	0.016	0.006	0.005	0.010
All U.S. LWRs	1.0	1.3	1.8	1.7	1.6	1.7
All U.S. PWRs	0.8	1.2	.3	1.4	1.3	1.3
All U.S. BWRs	1.3	1.6	2.7	2.3	2.3	2.8

8. UNUSUAL OCCURRENCES

8.1. INADVERTENT INSERTION OF RESERVE SHUTDOWN SYSTEM (RSS) MATERIAL INTO REGION 27

Surveillance of core performance data from June and July 1982 indicated that the reserve shutdown system (RSS) material may have been inadvertently released into region 27. The first evidence of the RSS material in region 27 came from examination of the region exit temperature and RPF distributions after the control rod was withdrawn from region 27 (i.e., control rod group 4B). It was noted that both the exit temperature and power in the north regions of the core was considerably higher than expected and the power in the south regions of the core was considerably lower than expected, with the largest effect in region 27.

Further examination of the measured data indicated:

- The orifice in region 27 was the most fully closed orifice in the core and the exit temperature was about the same as when the orifice was normally much more open.

- Steam generator module B-2-1 inlet temperature was lower than expected, and this module is fed by region 27.

- Fuel accountability analyses indicated a change in reactivity discrepancy of about 0.002 Δk. (This was subsequently determined to be the approximate reactivity worth of the RSS material in unrodded region 27.)

Subsequent RSS rupture disk pressure testing by PSC confirmed that, indeed, the RSS material had been inadvertently released into region 27.

A preliminary assessment of the consequences of continued short-term (4 to 6 weeks) operation with the RSS material in region 27 identified no immediate concerns. However, since it was about seven months before the next scheduled shutdown, a second assessment was made to evaluate the effects of operation for that period of time with the RSS in region 27. This evaluation included the following:

- Potential for boron migration out of RSS material.
- Potential for swelling of RSS material.
- Potential for mechanical stresses due to RSS material behaving as rigid column.
- Potential for agglomeration (due to formation of boric acid crystals) of RSS material.
- Effects of a moisture ingress incident on RSS material and impact on core performance.
- Evaluation of stresses in region 27 due to perturbed temperature distribution, swelling of RSS or mechanical binding (ratcheting).
- Effect on core reactivity.
- Long-term effect on power distributions and compliance with LCO 4.1.3.

The results of these analyses indicated that it was acceptable to continue plant operation at approximately 70% power with the RSS material

in region 27 for up to about 7 months. This conclusion was based on the assumption that the reactor was operated with low moisture levels.

While it was concluded that continued operation with the RSS material in region 27 was acceptable, one constraint was identified. This constraint resulted from the effects of the perturbed power distribution on the maximum worth control rod pair (region 11). The worth of the maximum worth rod exceeded that calculated without RSS material in region 27. The consequences of this increased control rod worth on the rod withdrawal accident were assessed and it was found that there were certain control rod configurations (positions) which could result in potential reactivity insertions greater than those analyzed in the design basis rod withdrawal accident. Therefore, limits on operating conditions were established to avoid the the potential for a reactivity insertion exceeding that analyzed in the design basis rod withdrawal accident. PSC operated the plant in accordance with these operating conditions until the plant was shut down on September 30, 1982, and the RSS material removed from region 27.

Details of these analyses are reported in Ref. 58.

8.2. CRACKED FUEL ELEMENT WEB

The cracked coolant hole web in two segment 8 standard fuel elements, detected during the post-irradiation examination of segment 2 elements, is discussed in Section 7.6.

8.3. POWER LEVEL UNCERTAINTY

Surveillance of core performance data during cycle 3 indicated that the reported thermal power was lower than the heat balance power. Further investigation, in cooperation with PSC, revealed that periodically during the cycle the core was inadvertently operated at higher than reported thermal power. Investigations and analyses by PSC (Ref. 61) and GA

concluded that the core overburn was the equivalent of about 7.5 EFPDs. These 7.5 EFPDs were subsequently incorporated into core performance analysis.

9. REFERENCES

1. FSV Fuels Engineering Staff, "Fort St Vrain Cycle 3 Core Performance Quarterly Report for Period Ending September 30, 1981," GA-C15822, September 1981.
2. FSV Fuels Engineering Staff, "Fort St. Vrain Cycle 3 Core Performance Quarterly Report for Period Ending December 31, 1981," GA-C15822, December 1981.
3. FSV Fuels Engineering Staff, "Fort St. Vrain Cycle 3 Core Performance Quarterly Report for Period Ending June 30, 1982," GA-C15822, June 1982.
4. FSV Fuels Engineering Staff, "Fort St. Vrain Cycle 3 Core Performance Quarterly Report for Period Ending September 30, 1982," GA-C15822, September 1982.
5. FSV Fuels Engineering Staff, "Fort St. Vrain Cycle 3 Core Performance Quarterly Report for Period Ending March 31, 1983," GA-C15822, March 1983.
6. FSV Fuels Engineering Staff, "Fort St. Vrain Cycle 3 Core Performance Quarterly Report for Period Ending September 30, 1983," GA-C15822, September 1983.
7. FSV Fuels Engineering Staff, "Fort St. Vrain Cycle 3 Core Performance Quarterly Report for Period Ending December 31, 1983," GA-C15822, December 1983.
8. FSV Fuels Engineering Staff, "Fort St. Vrain Cycle 3 Core Performance Quarterly Report for Period Ending March 31, 1984," GA-C15822, March 1984.
9. Malek, G. J., et al., "Investigations of the Fort St. Vrain Reactor Fluctuations," GA-C15369, September 1979.
10. "SAR for Fort St. Vrain Reload 1 Test Elements FTE-1 through FTE-8," GLP-5494, June 1977.

11. Malakhof, V., et al., "Segment 8 Design Support Document - Fort St. Vrain HTGR," GA-D16304, March 1981.
12. Malakhof, V., "Fuel Fabrication Acceptance Report - FSV Segment 8," GA-C16257, March 1981.
13. "Safety Analysis Report for Fuel Reload 2 - Cycle 3," GA-015812, April 1980.
14. Wagner, M. R., "GAUGE, A Two-Dimensional Few Group Neutron Diffusion-Depletion Program for a Uniform Triangular Mesh," GA-8307, March 1968.
15. FSV Fuels Engineering Staff, "Fort St Vrain Cycle 2 Core Performance Quarterly Report for the Period Ending June 30, 1981," GA-C15822, June 30, 1981.
16. Hackney, R., "FSV Cycle 3 Data for Reactivity Calculations and for Physics Surveillance Tests," GA Doc. 906047, July 1, 1981.
17. FSV Fuels Engineering Staff, "Fort St Vrain Cycle 1 Core Performance," GA-C15560, September 1979.
18. Hackney, R., "Fort St. Vrain Cycle 2 Core Performance," GA-C16743, April 1982.
19. Hoppes, D. F., et al., "The Effect of Nuclear Detector Decalibration on the Fort St. Vrain Reactor and Suggested Corrective Measures," GA-A13954, January 1978.
20. Kraetsch, H., and M. R. Wagner, "GATT - A Three-Dimensional Few Group Neutron Diffusion Theory Program for Hexagonal-Z Mesh," GA-8547, January 1969.
21. Malakhof, V., "FSV Cycle 3 Power History," GA Doc. 907731, November 19, 1984.
22. Malakhof, V., and W. Lefler, "Fuel Accountability at the End of Cycle 3," GA Doc. 907402, May 1984.
23. "End of Cycle 3 Fuel Accountability," Magnetic Tape Archive No. RPSD 3842, May 1984.
24. "Control Rod Management," EE-12-002, Issue A, December 1981.
25. Warembourg, D. W. (PSC) letter to G. Kuzmycz (NRC), "Fort St. Vrain Unit No. 1 Meeting, February 16, 1982 - RT-500K Testing," P-82036, February 9, 1982.
26. "Fluctuation Test Procedure, RT-500 Revision K," March 1981.

27. Hackney, R., "Fort St Vrain Testing and Analyses in Support of Long Term Full Power Operation," GA-C16937, to be issued.
28. Alberstein, D., and K. Asmussen, "Technical Specifications for Operation of FSV with Region Outlet Temperature Measurement Discrepancies," GA-C16781, June 1982.
29. "FSVCOR Input Instructions," GA Memo CNE:209:SM:80, November 10, 1980.
30. Burnette, R., "Test Status Report On Fort St. Vrain HTGR Coolant and Radiochemistry: July 1981 through June 1982," GA Doc. 906601, August 1982.
31. Burnette, R., "Test Status Report on Fort St. Vrain HTGR Coolant and Radiochemistry: July 1982 through June 1983," GA Doc. 907053, August 1983.
32. Burnette, R., "Test Status Report on Fort St. Vrain HTGR Coolant and Radiochemistry: July 1983 through June 1984, GA Doc. 907650, September 1984.
33. Burnette, R. D., "Radiochemical Analysis of the First Plateout Probe from the Fort St. Vrain HTGR," GA-A16764, June 1982.
34. Dunn, T. D., "Fort St. Vrain Core Support Block Oxidation Analyses for Plant Operation from June 1976 to February 1979," GA-D15571, September 1979.
35. Hoot, C. G., and S. C. Bachelor, "Fort St. Vrain Core Support Block Oxidation Analyses for Plant Operation from June 1976 through June 1980," GA-C16158, January 1981.
36. Dunn, T. D., et al., "CSBBO-3: A Computer Program for Analysis of FSV Core Support Block Oxidation Distribution - Program Description and Users Manual," GA-D15577, October 1977.
37. Boltinghouse, S. T., et al., "Fort St. Vrain Core Support Block Analysis for Plant Operation from July 1980 to December 1982," GA Doc. 907410, April 1984.
38. Richards, M., "FSV CSB Oxidation Due to Water Ingress Transient from 6/22/84 to 6/23/84," GA Doc. 907622, September 1984.
39. Dunn, T. D., "Modification of the CSBBO-3 Computer Code," GA Doc. 906172, August 1981.

40. Dunn, T., and J. Battaglia, "Prediction of Graphite Burnoff in FSV Surveillance Samples - Cycle 2," GA Doc. 906223, September 25, 1981.

41. "Test Specification for PIE of PGX Surveillance Specimens (Region 25)," GA Doc. 906223/A, September 25, 1981.

42. Beanan, L. A., "Results of PGX Graphite Surveillance Fort St. Vrain Region 25," GA Doc. 906624, October 21, 1982.

43. Saurwein, J. J., "Nondestructive Examination of 54 Fuel and Reflector Elements from Fort St. Vrain Core Segment 2," GA-A16829, October 1982.

44. Ketterer, J. W., "Visual Examination Results of Segment 2 FSV Fuel Elements 1-2415, 1-0172, 2-2693, 1-0108 and 5-0801," GA Doc. 906577/2, April 1983.

45. McCord, F., "Postirradiation Examination and Evaluation of FSV Fuel Element 1-2415," GA Doc. 907079, November 7, 1984.

46. Yu, H., et al., "Seismic Strength of the FSV Cracked Block," GA Doc. 907429, July 10, 1984.

47. Ho, F., "FSV-Structural Test of H-327 Elements with Simulated Cracks," GA Doc. 907428, April 24, 1984.

48. Kapernick, R., "Operating History of the FSV Cracked Blocks," GA Doc. 906811, February 25, 1983.

49. "Structural Integrity of HTGR Fuel Elements," GA Doc. PC-000045, June 30, 1982.

50. Smith, P. D., "SURVEY/STRESS, A Model to Calculate Irradiation-Induced Stresses, Strains, and Deformations in an HTGR Fuel Block Using Visoelastic Beam Theory," GA-A13712, October 20, 1975.

51. McCord, F., "Nondestructive Examinations of 62 Fuel and Reflector Elements from Fort St. Vrain Core Segment 3," GA Doc. 907785, January 24, 1985.

52. Hackney, R., and J. Saeger, "Investigations of the Fort St. Vrain Cycle 2 Reactor Fluctuations Through October 26, 1979," GA-C15767, March 1980.

53. Hackney, R., and W. Breher, "Investigations of the Fort St Vrain Reactor Fluctuations - January-March 1979," GA-C15536, August 1979.

54. Asmussen, K., et al., "Core Testing and Operation of Fort St. Vrain Up to 100% Power," GA-C16701, June 1982.

55. NUREG-0173, Vol. 3.

56. Brooks, B. G., NRC.

57. Inside NRC, Vol. 18, September 1984.

58. Asmussen, K., "Effects on FSV Core of Operating with Reserve Shutdown Material in Region 27," GA Doc. 906618, June 1983.

59. Disselhorst, B. F., et al., "Fort St. Vrain Fuel Element Quality Control," GA-D13772, December 31, 1975.

60. Lefler, W., "Support Analysis for FSV SR 5.1.7 - December 1983," GA Doc. 907240, February 17, 1984.

61. November Operating Report for Period 11/1/83 thru 11/30/83, Docket No. 59-267, December 12, 1983.

62. Hudritsch, W. W., V. Jovanovic, and D. L. Georghiou, "SURVEY, A Computer Code for the Thermal and Fuel Performance Analysis of High-Temperature Gas-Cooled Reactor," GA-C17554, March 1984.

63. Smith, P. D., "TRAFIC, A Computer Program for Calculating the Release of Metallic Fission Products from an HTGR Core," GA-A14721, February 1978.

64. Jovanovic, V., "FSV Fuel Performance Analysis for the First Three Cycles," GA Doc. 907715, June 28, 1985.

65. Myers, B. F., "Fuel Design Data Manual," GA Doc. 901866/E, September 28, 1984.

66. Goodin, D. T., "FSV Fuel Performance," GA Doc. 18-R-59/3, August 1, 1984.

67. Ketterer, J., "Reference HTGR Fuel Compact Thermal Conductivity Data Base and Model," GA Doc. 907591, Issue N/C, August 29, 1985.

68. Wan, M., "Core Performance Calculations for the First Two Cycles of the FSV Core," GA Doc. 906274/1, September 25, 1981.

69. Wan, M., "Cesium and Strontium Release Calculations for the First Two Cycles of the FSV Core," Memo CNE:194:MW:81, October 9, 1981.

70. Ketterer, J. W., and K. E. Partain, "Capsules HRB-17/-18 Preirradiation Report," GA Doc. 906975/1, August 1983.

71. Goodin, D. T., "FSV Fuel Performance," GA Doc. 18-R-59, Issue N/C, May 13, 1985.

72. Montgomery, F., "Test Report on Hydrolysis of HTGR Carbide Fuels: Chemical Reactions and Consequences," GA Doc. 904929/1, September 26, 1980.

73. Montgomery, F., "Gamma Scanning of FSV Core Segment 3 Fuel Elements," GA Doc. 908043, July 8, 1985.